New Phytologist

New insights into the mechanisms of plant isotope fractionation from combined analysis of intramolecular ^{13}C and deuterium abundances in *Pinus nigra* tree-ring glucose

Thomas Wieloch[1,2], Meisha Holloway-Phillips[3], Jun Yu[4] and Totte Niittylä[1]

[1]Department of Forest Genetics and Plant Physiology, Swedish University of Agricultural Sciences, Umeå Plant Science Centre, 90183, Umeå, Sweden; [2]Division of Geological and Planetary Sciences, California Institute of Technology, 91125 Pasadena, CA, USA; [3]Research Unit of Forest Dynamics, Swiss Federal Institute for Forest, Snow and Landscape Research WSL, 8903, Birmendsorf, Switzerland; [4]Department of Mathematics and Mathematical Statistics, Umeå University, 90187, Umeå, Sweden

Author for correspondence:
Thomas Wieloch
Email: thomas.wieloch@slu.se

Received: *17 June 2024*
Accepted: *20 August 2024*

New Phytologist (2025) **245:** 1000–1017
doi: 10.1111/nph.20113

Key words: carbon stable isotopes, hydrogen stable isotopes, intramolecular isotope analysis, isotope fractionation mechanisms, leaf water status, plant–environment interactions, stem water status, tree rings.

Summary

- Understanding isotope fractionation mechanisms is fundamental for analyses of plant ecophysiology and paleoclimate based on tree-ring isotope data.
- To gain new insights into isotope fractionation, we analysed intramolecular ^{13}C discrimination in tree-ring glucose (Δ_i', i = C-1 to C-6) and metabolic deuterium fractionation at H^1 and H^2 (ε_{met}) combinedly. This dual-isotope approach was used for isotope-signal deconvolution.
- We found evidence for metabolic processes affecting Δ_1' and Δ_3', which respond to air vapour pressure deficit (*VPD*), and processes affecting Δ_1', Δ_2', and ε_{met}, which respond to precipitation but not *VPD*. These relationships exhibit change points dividing a period of homeostasis (1961–1980) from a period of metabolic adjustment (1983–1995). Homeostasis may result from sufficient groundwater availability. Additionally, we found Δ_5' and Δ_6' relationships with radiation and temperature, which are temporally stable and consistent with previously proposed isotope fractionation mechanisms.
- Based on the multitude of climate covariables, intramolecular carbon isotope analysis has a remarkable potential for climate reconstruction. While isotope fractionation beyond leaves is currently considered to be constant, we propose significant parts of the carbon and hydrogen isotope variation in tree-ring glucose originate in stems (precipitation-dependent signals). As basis for follow-up studies, we propose mechanisms introducing Δ_1', Δ_2', Δ_3', and ε_{met} variability.

Introduction

Analysis of the systematic $^{13}C/^{12}C$ variation (commonly termed '^{13}C signal'; abbreviations in Table 1) across tree-ring series is widely used to study past climate conditions, plant–environment interactions, and physiological traits such as leaf water-use efficiency (CO_2 uptake relative to H_2O loss) (Leavitt & Roden, 2022). Signals found at the whole-tissue or whole-molecule level (Fig. 1a, top and middle) are commonly interpreted based on a simplified mechanistic model of ^{13}C discrimination, Δ (denoting $^{13}C/^{12}C$ variation caused by physiological processes) (Farquhar *et al.*, 1982). This model considers isotope effects of CO_2 diffusion from ambient air into intercellular air spaces (Craig, 1953) and CO_2 assimilation by rubisco (Roeske & O'Leary, 1984) and phospho*enol*pyruvate carboxylase (PEPC; Fig. 2) (Farquhar, 1983; Farquhar & Richards, 1984). Manifestation of these effects as ^{13}C discrimination depends on the ratio of intercellular-to-ambient CO_2 partial pressure ($p_i : p_a$) (Farquhar *et al.*, 1982), and a highly significant positive relationship between $p_i : p_a$ and leaf Δ was confirmed experimentally (Evans *et al.*, 1986). Environmental parameters influence $p_i : p_a$ and thus leaf Δ (Evans *et al.*, 1986) by affecting the stomatal aperture and CO_2 assimilation. For instance, in response to drought, isohydric plant species such as *Pinus nigra* (studied here) close their stomata (McDowell *et al.*, 2008). This can be expected to decrease $p_i : p_a$ and leaf Δ (Farquhar *et al.*, 1982; Evans *et al.*, 1986).

Isotope fractionation by metabolic processes downstream of CO_2 assimilation is complex (Hobbie & Werner, 2004), incompletely understood (Badeck *et al.*, 2005; Cernusak *et al.*, 2009), and has yet to be adequately integrated into ^{13}C-discrimination models (Ubierna *et al.*, 2022). Specifically, the simplified ^{13}C discrimination model described above requires multiple adaptations to enable correct interpretation of the ^{13}C composition of tree-ring glucose (studied here). For instance, we recently argued that incorporation of carbon assimilated by PEPC into tree-ring glucose is negligible because leaves lack a high-flux pathway shuttling this carbon into glucose metabolism (Fig. 2; Wieloch *et al.*, 2022c). Therefore, all carbon in tree-ring glucose proposedly derives from rubisco-assimilated CO_2. Rubisco catalyses the

Table 1 Abbreviations and symbols.

Abbreviation	Definition
^{13}C signal	Systematic $^{13}C/^{12}C$ variation
DAHPS	3-Deoxy-D-*arabino*-heptulosonate-7-phosphate synthase
F6P	Fructose 6-phosphate
G6P	Glucose 6-phosphate
G6PD	Glucose-6-phosphate dehydrogenase
GAP	Glyceraldehyde 3-phosphate
GAPDH	Glyceraldehyde-3-phosphate dehydrogenase
NMRS	Nuclear magnetic resonance spectroscopy
OPPP	Oxidative branch of the pentose phosphate pathway
PEP	Phospho*enol*pyruvate
PEPC	Phospho*enol*pyruvate carboxylase
PGA	3-Phosphoglycerate
PGI	Phosphoglucose isomerase
PK	Pyruvate kinase
RuBP	Ribulose 1,5-bisphosphate
TCAC	Tricarboxylic acid cycle

Symbol	Definition
p_a	Ambient CO_2 partial pressure
p_i	Intercellular CO_2 partial pressure
PRE	Precipitation
RAD	Global radiation
SD	Sunshine duration
$SPEI_i$	Standardised precipitation-evapotranspiration index calculated for different timescales, $i = 1, 3, 6, 8, 12, 16, 24, 36, 48$ months
TMP	Air temperature
VPD	Air vapour pressure deficit
Δ	^{13}C discrimination denoting $^{13}C/^{12}C$ variation due to plant physiological processes
Δ_i'	Intramolecular ^{13}C discrimination where *i* denotes individual glucose carbon positions and the prime denotes data corrected for ^{13}C signal redistribution by heterotrophic triose phosphate cycling
Δ_{1-2}'	Arithmetic average of Δ_1' and Δ_2'
Δ_{1-3}'	Arithmetic average of Δ_1', Δ_2', and Δ_3'
Δ_{5-6}'	Arithmetic average of Δ_5' and Δ_6'
ϵ_{met}	Metabolic deuterium fractionation at glucose H^1 and H^2

addition of CO_2 to ribulose 1,5-bisphosphate (RuBP). Since this reaction is essentially the sole carbon source of glucose, ^{13}C discrimination accompanying CO_2 diffusion and subsequent rubisco CO_2 assimilation (denoted diffusion–rubisco discrimination) is expected to affect all glucose carbon positions equally (Wieloch *et al.*, 2018, 2022c).

Moreover, we recently measured Δ intramolecularly at all six carbon positions, *i*, of glucose (Fig. 1a, bottom) extracted across an annually resolved tree-ring series of *P. nigra* (Wieloch *et al.*, 2018). The resultant Δ_i' data set comprises 6×31 values (study period: 1961–1995; four years missing: 1977, 1978, 1981, 1982), which were corrected for ^{13}C signal redistribution by heterotrophic triose phosphate cycling (indicated by prime, Supporting Information Notes S1). We found that, at least, four ^{13}C signals contribute to the interannual $^{13}C/^{12}C$ variability in tree-ring glucose (Fig. 1b) and proposed the following theories on underlying mechanisms.

We initially proposed the diffusion–rubisco signal is preserved at C-1 to C-3 (Figs 1b, 2; Wieloch *et al.*, 2018); although this view is modified here. Additionally, C-1 and C-2 are thought to carry ^{13}C signals due to fractionation at phosphoglucose isomerase (PGI has carbon isotope effects at both C-1 and C-2) and glucose-6-phosphate dehydrogenase (G6PD has a carbon isotope effect at C-1) (Wieloch *et al.*, 2018, 2022a). Two leaf-level mechanisms of signal introduction were proposed. First, with decreasing carbon assimilation, the PGI reaction in chloroplasts moves from being on the side of fructose 6-phosphate (F6P) towards equilibrium (Fig. 2; Dietz, 1985). This shift is expected to cause ^{13}C enrichments at C-1 and C-2 of glucose 6-phosphate (G6P) and its derivatives starch and tree-ring glucose (Table 2; Wieloch *et al.*, 2018). Moreover, shifts towards PGI equilibrium are associated with G6P increases (Dietz, 1985). Increasing G6P is thought to cause G6PD activation and thus increasing flux through the oxidative pentose phosphate pathway (OPPP) in chloroplasts (Cossar *et al.*, 1984; Sharkey & Weise, 2016; Preiser *et al.*, 2019) resulting in additional ^{13}C enrichment at C-1 of

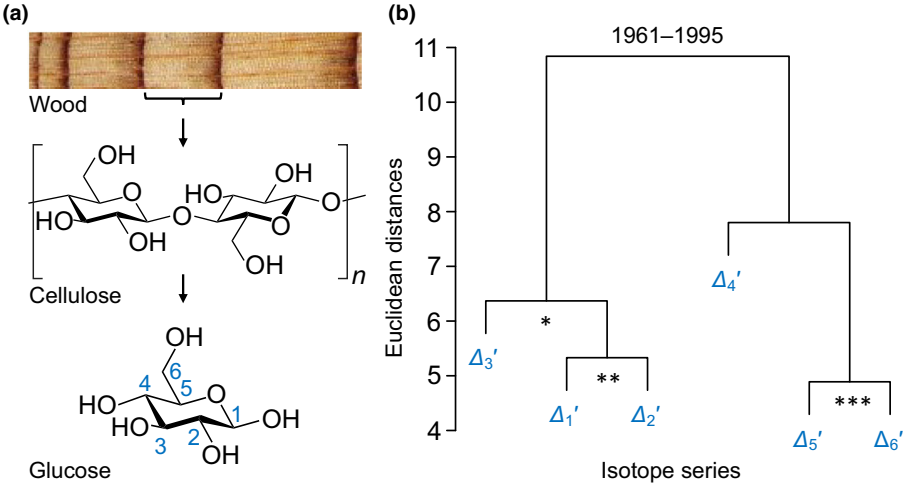

Fig. 1 Carbon isotope discrimination in tree rings. (a) Levels of resolution of stable carbon isotope analysis: whole plant materials, whole molecules, intramolecular carbon positions. (b) Hierarchical clustering of Δ_i' series for the period 1961–1995. Significance of series correlation: *, $P \leq 0.05$; **, $P \leq 0.01$; ***, $P \leq 0.001$. Modified figure from Wieloch *et al*. (2018). Δ_i' denotes intramolecular ^{13}C discrimination in glucose extracted across an annually resolved *Pinus nigra* tree-ring series.

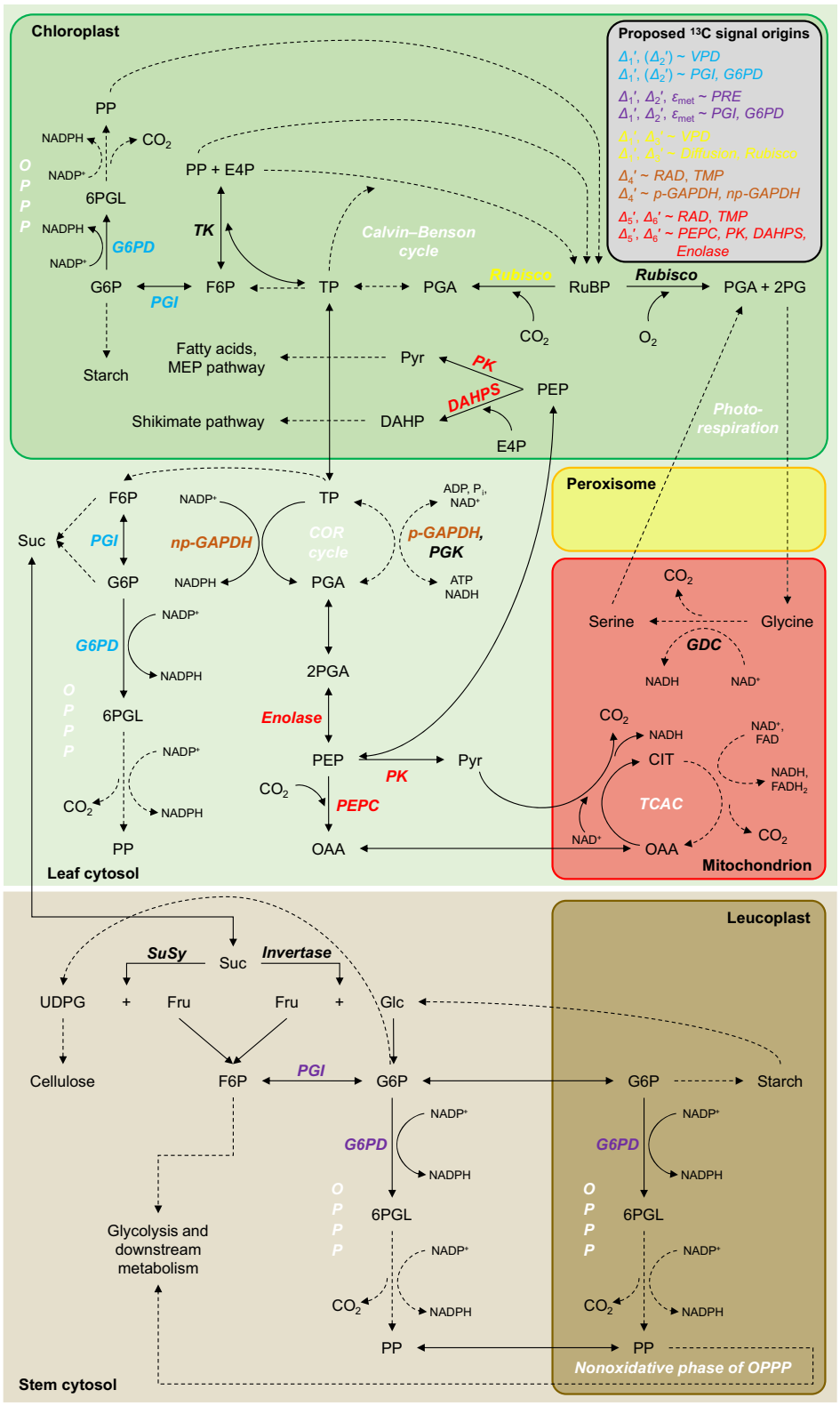

Fig. 2 Proposed metabolic origins of carbon and hydrogen isotope signals in tree-ring glucose. Dashed arrows indicate that intermediate reactions are not shown. 2PG, 2-phosphoglycolate; 2PGA, 2-phosphoglycerate; 6PGL, 6-phosphogluconolactone; ADP, adenosine diphosphate; ATP, adenosine triphosphate; CIT, citrate; COR cycle, cytosolic oxidation–reduction cycle; DAHP, 3-deoxy-D-*arabino*-heptulosonate 7-phosphate; DAHPS, DAHP synthase; E4P, erythrose 4-phosphate; F6P, fructose 6-phosphate; FAD, flavin adenine dinucleotide; Fru, fructose; G6P, glucose 6-phosphate; G6PD, G6P dehydrogenase; GDC, glycine decarboxylase complex; Glc, glucose; MEP pathway, methylerythritol 4-phosphate pathway; NAD^+, nicotinamide adenine dinucleotide; $NADP^+$, nicotinamide adenine dinucleotide phosphate; np-GAPDH, non-phosphorylating glyceraldehyde-3-phosphate dehydrogenase; OAA, oxaloacetate; OPPP, oxidative pentose phosphate pathway; PEP, phospho*enol*pyruvate; PEPC, PEP carboxylase; PGA, 3-phosphoglycerate; p-GAPDH, phosphorylating glyceraldehyde-3-phosphate dehydrogenase; PGI, phosphoglucose isomerase; PGK, phosphoglycerate kinase; P_i, inorganic phosphate; PK, pyruvate kinase; PP, pentose phosphate; *PRE*, precipitation; Pyr, pyruvate; *RAD*, global radiation; Rubisco, ribulose-1,5-bisphosphate carboxylase/oxygenase; RuBP, ribulose 1,5-bisphosphate; Suc, sucrose; SuSy, sucrose synthase; TCAC, tricarboxylic acid cycle; TK, transketolase; *TMP*, air temperature; TP, triose phosphates (glyceraldehyde 3-phosphate, dihydroxyacetone phosphate); UDPG, uridine diphosphate glucose; *VPD*, air vapour pressure deficit; Δ_i', intramolecular ^{13}C discrimination where *i* denotes individual glucose carbon positions and the prime denotes data corrected for ^{13}C signal redistribution by heterotrophic triose phosphate cycling; ε_{met}, metabolic deuterium fractionation at glucose H^1 and H^2.

G6P and its derivatives (Wieloch *et al.*, 2022a). Hydrogen isotope evidence consistent with these proposed metabolic shifts was reported recently (Wieloch *et al.*, 2022a). Second, the PGI reaction in chloroplasts is usually displaced from equilibrium on the side of F6P, whereas the PGI reaction in the cytosol is closer to or in equilibrium (Dietz, 1985; Gerhardt *et al.*, 1987; Leidreiter *et al.*, 1995; Schleucher *et al.*, 1999; Szecowka *et al.*, 2013). This is expected to result in $^{13}C/^{12}C$ differences between starch and

Table 2 Hydrogen isotope effects of phosphoglucose isomerase (PGI, Rose & O'Connell, 1961), and carbon isotope effects of glucose isomerase (GI, Gilbert *et al*., 2012).

PGI, $\alpha = k_H/k_D$			GI, $\alpha = k_{^{12}C}/k_{^{13}C}$				
F6P, H^{1R}		G6P, H^2	F6P, C-1	F6P, C-2		G6P, C-1	G6P, C-2
	→	$2.\overline{2}$			→	1.005	1.015
0.9	↔	$1.\overline{1}$	1.013	0.993	↔	0.987	1.007
2	←		1.018	1.008	←		

→, kinetic isotope effect of the forward reaction; ←, kinetic isotope effect of the backward reaction; ↔, equilibrium isotope effect. Calculated values underlined. Since GI and PGI have the same reaction mechanism, the ^{13}C isotope effects of GI and PGI are thought to be very similar (Gilbert *et al*., 2012). H^{1R}, *pro-R* hydrogen at F6P C-1.

sucrose at both hexose C-1 and C-2 (Table 2; Wieloch *et al*., 2022b). By extension, changes in the relative contribution of starch to the biosynthesis of tree-ring glucose is expected to contribute to the ^{13}C signals at C-1 and C-2.

In addition to ^{13}C signals at C-1 and C-2, tree-ring glucose samples discussed here carry deuterium signals caused by metabolic processes at H^1 and H^2. These signals are strongly correlated and were approximated as:

$$\varepsilon_{met} = \frac{(D_1 + D_2)/2}{(D_3 + D_4 + D_5 + D_{6S} + D_{6R})/5} - 1 \qquad \text{Eqn 1}$$

where D_i denotes relative deuterium abundances at individual H-C positions (Wieloch *et al*., 2022a,b). Variability of ε_{met} pertaining to glucose H^1 and H^2 was attributed to isotope effects of G6PD ($k_H/k_D = 2.97$) (Hermes *et al*., 1982) and PGI (Table 2; Rose & O'Connell, 1961; Wieloch *et al*., 2022a,b), respectively. Proposedly, G6PD and PGI-dependent metabolic processes in both leaves and tree rings may contribute to ε_{met} signal introduction (Wieloch *et al*., 2022b). Interestingly, Wacker (2022) recently reported that the commonly observed whole-molecule deuterium depletion of leaf starch that derives from deuterium depletion at starch glucose H^2 (Schleucher *et al*., 1999; Wieloch *et al*., 2022a) is not detectable in nocturnal sucrose. Proposedly, this depletion is either washed out at the level of cytosolic PGI or masked either by the vacuolar sucrose pool or deuterium enrichments at other sucrose hydrogen positions. Washout would imply that any ε_{met} signal present at leaf-level G6P H^2 is lost to the medium. In this case, the ε_{met} signal at tree-ring glucose H^2 may originate outside leaves.

At tree-ring glucose C-4 (Fig. 1b), the diffusion–rubisco ^{13}C signal is thought to be absent due to counteracting fractionation by leaf-cytosolic glyceraldehyde-3-phosphate dehydrogenases (GAPDH; Fig. 2) (Wieloch *et al*., 2021). Signal removal may involve both changes in 3-phosphoglycerate (PGA) flux into downstream metabolism including the tricarboxylic acid cycle (TCAC) relative to flux into tree-ring glucose and changes in flux through the cytosolic oxidation–reduction cycle (Wieloch, 2021; Wieloch *et al*., 2021).

The ^{13}C signal at C-5 and C-6 (Fig. 1b) is thought to derive from the postulated (but not yet measured) isotope effects of leaf-level enzymes that modify the carbon double bond in phospho*enol*pyruvate (PEP, Fig. 2) (Wieloch *et al*., 2022c). This includes enolase, pyruvate kinase (PK), PEPC, and 3-deoxy-D-*arabino*-heptulosonate-7-phosphate synthase (DAHPS), the first enzyme of the shikimate pathway. Breaking the double bond in PEP is thought to proceed faster when ^{12}C instead of ^{13}C forms this bond (Wieloch *et al*., 2022c). Consequently, increasing relative flux into metabolism downstream of PEP is thought to ^{13}C enrich remaining PEP at the double-bond carbons and their derivatives including glucose C-5 and C-6 (Wieloch *et al*., 2022c). For example, O_3 causes downregulation of rubisco, upregulation of PEPC, and DAHPS expression (Dizengremel, 2001; Janzik *et al*., 2005; Betz *et al*., 2009). This is expected to cause increasing relative flux into metabolism downstream of PEP (Wieloch *et al*., 2022c). Accordingly, we previously found a negative relationship between reconstructed tropospheric O_3 concentration and tree-ring glucose Δ_{5-6}' (arithmetic average of Δ_5' and Δ_6', Table 1) (Wieloch *et al*., 2022c).

By contrast, the diffusion–rubisco signal is not evident at C-5 and C-6 (Wieloch *et al*., 2022c). This was explained (*inter alia*) by interaction between photorespiration and the TCAC (Fig. 2; Wieloch *et al*., 2022c). Photorespiration increases with drought, which results in increasing supply of mitochondrial NADH via the glycine decarboxylase complex. Since this NADH can feed oxidative phosphorylation, NADH and $FADH_2$ supply by the TCAC, which requires injection of PEP into the TCAC via PK and PEPC, may be reduced. This should result in Δ_{5-6}' increases counteracting drought-induced decreases in diffusion–rubisco discrimination (as mentioned in the first section).

The theories of isotope signal introduction outlined above require further testing. They derive from separate analyses of either the Δ_i' or deuterium data set. However, some reactions exhibit both carbon and hydrogen isotope effects (e.g. G6PD at G6P C-1 and H^1; PGI at G6P C-1, C-2, and H^2 but not H^1) and should therefore introduce intercorrelated ^{13}C and deuterium signals (suggested terminology: hydro-carbon isotope signals and hydro-carbon isotope fractionation). Combined analysis of intramolecular ^{13}C and deuterium data can, in principle, help to separate those signals from signals introduced by reactions, which merely exhibit either carbon or hydrogen isotope effects. Therefore, we here studied the relationships between Δ_i' and ε_{met} and their dependence on environmental parameters. Based on our results, we critically examine and revise existing isotope theory and provide new insights into a central open question – whether

carbon and hydrogen isotope variability across tree rings derives from leaf-level processes only (as supported by current evidence) or whether processes in the stem contribute as well.

Materials and Methods

Isotope data

The Δ_i' and ε_{met} data sets of *P. nigra* Arnold reanalysed here are described in Wieloch *et al.* (2018, 2022b) and in Notes S1. Δ may be affected by p_a (Schubert & Jahren, 2012). Annual p_a data were obtained for the Mauna Loa Observatory, HI (curators: Pieter Tans, NOAA/ESRL, Boulder, USA; Ralph Keeling, Scripps Institution of Oceanography, La Jolla, USA). However, we found no significant correlation between Δ and p_a ($r = -0.32$, $P > 0.05$, $n = 31$). Moreover, in line with the mechanistic model of diffusion–rubisco ^{13}C discrimination (Farquhar *et al.*, 1989), most previous studies have reported positive slopes for the regression of these variables (Schubert & Jahren, 2012), but we found a negative slope (-0.02 ± 0.01SE). Hence, in the present case, the effect of p_a on Δ is not verifiable. Therefore, we neither correct Δ nor Δ_i' for p_a.

Estimation of ε_{met} according to Eqn 1 aims to remove fractionation by nonmetabolic processes such as leaf water deuterium enrichment (Wieloch *et al.*, 2022b). Series of ε_{met} calculated separately for H^1 and H^2 (by replacing the numerator in Eqn 1 with D_1 and D_2, respectively) are essentially perfectly correlated considering that both series exhibit significant random variation due to the relatively large error of NMRS measurements (1983–1995, $r = 0.92$, $P = 10^{-5}$, $n = 13$).

Climate data

Data of relative humidity, precipitation (*PRE*), global radiation (*RAD*), sunshine duration (*SD*), and air temperature (*TMP*) are from the climate station Hohe Warte (Vienna, Austria, 48.23°N, 16.35°E, 198 m amsl) (Klein Tank *et al.*, 2002). Air vapour pressure deficit (*VPD*) was calculated following published procedures (Abtew & Melesse, 2013). Data of the standardised precipitation-evapotranspiration index ($SPEI_i$) calculated for integrated periods of $i = 1$, 3, 6, 8, 12, 16, 24, 36, 48 months were obtained for 48.25°N, 16.25°E (Fan & van den Dool, 2004; Beguería *et al.*, 2010). The SPEI is a multiscalar drought index approximating soil moisture variability when calculated for short timescales and groundwater variability when calculated for long timescales (Vicente-Serrano *et al.*, 2010). The *RAD* series starts in 1964 while all other climate series start in 1961. Horizontal distances between the tree site and the climate station and grid point are < 15 km. Vertical offsets are small. Hence, climate data and site conditions are expected to be in good agreement.

Data analysis

Based on *TMP* during the study period (1961–1995), the growing season at the site was estimated to extend from March to November (Wieloch *et al.*, 2018). Conifers form tree rings over the course of several months (Cuny *et al.*, 2014). Therefore, all statistical analyses exclusively consider periods comprising ≥ 4 growing season months. According to autocorrelation analyses on Δ_i' and Δ series, the growth of the trees studied here has not been significantly affect by interannual carry-over of carbon (Wieloch *et al.*, 2018). Therefore, our statistical analyses do not consider the climate conditions of previous years.

After mean-centring and unit-variance scaling of Δ_i' series, hierarchical cluster analysis was done with the functions dist() and hclust() of the STATS package in R (R Core Team, 2021), choosing Euclidean distances and Ward's fusion criterion as inputs (Ward, 1963). Pearson's correlation analysis, ordinary least squares regression analysis, and Shapiro–Wilk normality tests were respectively done with the functions cor(), lm(), and shapiro.test() of the STATS package in R (R Core Team, 2021). The fraction of systematic variance in isotope series was estimated according to published procedures (Nilsson *et al.*, 1996). Change point tests were done with the function detectChangePointBatch() of the CPM package in R (parametric generalised likelihood ratio test and nonparametric Lepage test) (Ross, 2015). *F*-tests and one-tailed *t*-tests were, respectively, done with the functions f.test() and t.test() in EXCEL (Microsoft Corp., Redmond, WA, USA).

Results

Hydro-carbon isotope signals at tree-ring glucose HC-1 and HC-2

Tree-ring glucose of our *P. nigra* samples exhibits strongly correlated hydrogen isotope signals at H^1 and H^2 (Wieloch *et al.*, 2022b). These signals occur only after crossing a change point in 1980. Isotope–environment relationship analyses indicated that the trees had likely access to groundwater before 1980, which prevented changes in the processes introducing these isotope signals. We proposed the signals derive from the hydrogen isotope effects of G6PD ($k_H/k_D = 2.97$) (Hermes *et al.*, 1982) and PGI (Table 2; Rose & O'Connell, 1961; Wieloch *et al.*, 2022a) in autotrophic and/or heterotrophic tissue (Fig. 2; see the Introduction section) (Wieloch *et al.*, 2022a,b). If this proposal is correct then there should be related signals in Δ_1' and Δ_2' due to the carbon isotope effects of G6PD affecting C-1 ($k_{^{12}C}/k_{^{13}C} = 1.0165$) (Hermes *et al.*, 1982) and PGI affecting C-1 and C-2 (Table 2; Gilbert *et al.*, 2012). Several findings support this hypothesis. First, among all Δ_i' series, Δ_1', Δ_{1-2}', Δ_{1-3}', and Δ are not normally distributed (Table S1, negative skew). Second, among these non-normal series, Δ_{1-2}', Δ_{1-3}', and Δ exhibit a change point in 1980 (Δ_{1-2}': parametric test, $P < 0.001$, nonparametric test, $P < 0.05$; Δ_{1-3}': parametric test, $P < 0.01$; Δ: parametric test: $P < 0.05$; $n = 31$). Third, 1983–1995 average values of Δ_1', Δ_2', Δ_{1-2}', and Δ are significantly lower than the average values of 1961–1980, while the 1983–1995 variance is significantly larger (Table S2). By contrast, Δ_3' does not exhibit significant differences in average value or variance between the two periods. Fourth, Δ_1' and Δ_2' data pertaining to 1983–1995 are significantly correlated ($r = 0.67$, $P = 0.01$, $n = 13$). Fifth, ε_{met} approximates average hydrogen isotope fractionation at glucose H^1 and H^2 caused by metabolic processes

(Eqn 1). Using simple linear regression modelling, we found significant negative relationships between the 1983–1995 data of ε_{met} and $\Delta_1{}'$ as well as $\Delta_2{}'$, but not $\Delta_3{}'$ or any other $\Delta_i{}'$ (Fig. 3, green circles; $\Delta_1{}' \sim \varepsilon_{met}$: $R^2 = 0.35$, adj$R^2 = 0.29$, $P = 0.03$; $\Delta_2{}' \sim \varepsilon_{met}$: $R^2 = 0.54$, adj$R^2 = 0.50$, $P = 0.004$; $\Delta_3{}' \sim \varepsilon_{met}$: $R^2 = 0.21$, adj$R^2 = 0.13$, $P > 0.1$; $n = 13$; Table S3). Our ^{13}C-NMRS data exhibit relatively large measurement errors. Based on estimates of this random error variance, *c.* 88% of the variance in the $\Delta_1{}'$ and $\Delta_2{}'$ data of 1983–1995 is systematic variance (Table S4). Hence, *c.* 33% and 57% of the systematic variance in $\Delta_1{}'$ and $\Delta_2{}'$ is explained by processes causing ε_{met} variation (0.29/0.88 and 0.5/0.88) while *c.* 67% and 43%, respectively, go back to other processes. Taken together, carbon and hydrogen isotope signals at glucose HC-1 and HC-2 are significantly associated during 1983–1995 but not during 1961–1980 (Notes S2). The processes introducing these signals cause concerted ^{13}C and deuterium enrichments (Fig. 3a,b).

Isotope–environment relationships at tree-ring glucose C-1 to C-3

As evident from our previously published hierarchical cluster analysis and Pearson's correlation analyses for the whole period (1961–1995), $\Delta_1{}'$, $\Delta_2{}'$, and $\Delta_3{}'$ share common variability (Fig. 1b; Wieloch *et al.*, 2018). Since $\Delta_{1-2}{}'$ and $\Delta_{1-3}{}'$ exhibit change points in 1980 (as mentioned in the previous section and Tables S1, S2), we analysed the early (1961–1980) and late period (1983–1995) separately.

During the late period, $\Delta_1{}'$ and $\Delta_3{}'$ are more closely associated (Fig. 4a; $r = 0.87$, $P = 10^{-4}$, $n = 13$) than $\Delta_1{}'$ and $\Delta_2{}'$ ($r = 0.67$, $P = 0.01$, $n = 13$). While this contrasts with results for the whole period (Fig. 1b), it is consistent with isotope–climate relationship patterns for the late period. $\Delta_1{}'$ and $\Delta_3{}'$ correlate similarly with numerous climate parameters and periods (Table 3; *VPD*, *PRE*, *SPEI*$_1$ to *SPEI*$_{16}$, *TMP*, *SD*). By contrast, $\Delta_2{}'$ correlates only with one *VPD* period and several *PRE* periods. A model including ε_{met} and growing season *VPD* as cofactors captures most of the systematic variance in $\Delta_1{}'$ of 88% (Tables 4 (M1), S4). Consistent with the findings described earlier (Fig. 3; Table 3), only ε_{met} but not growing season *VPD* contributes significantly to the $\Delta_2{}'$ model, whereas only growing season *VPD* but not ε_{met} contributes significantly to the $\Delta_3{}'$ model (Table 4 (M2, M3)). Removing insignificant terms, we find that ε_{met} explains 57% of the systematic variance in $\Delta_2{}'$, while growing season *VPD* explains the entire systematic variance in $\Delta_3{}'$ (Tables 4 (M4, M5), S4). The effect of *VPD* on $\Delta_1{}'$ is about twice as large as on $\Delta_3{}'$ (Table 4 (M1 vs M5)) while the effect of ε_{met} on $\Delta_1{}'$ is about half as large as on $\Delta_2{}'$ (M1 vs M4). Intriguingly, $\Delta_1{}'$ and $\Delta_3{}'$ are affected by processes that respond to growing season *VPD*. *VPD*-dependent processes can account for both the clustering and correlation between $\Delta_1{}'$ and $\Delta_3{}'$ data of 1983–1995 (Fig. 4a). By contrast, ε_{met} is significantly correlated only with *PRE* (especially March–July *PRE*) but no other climate parameter (Tables 4 (M11), S5). Furthermore, in our $\Delta_1{}'$ and $\Delta_2{}'$ models, ε_{met} can be substituted by March–July *PRE* (Table 4 (M1 vs M6, M4 vs M7)).

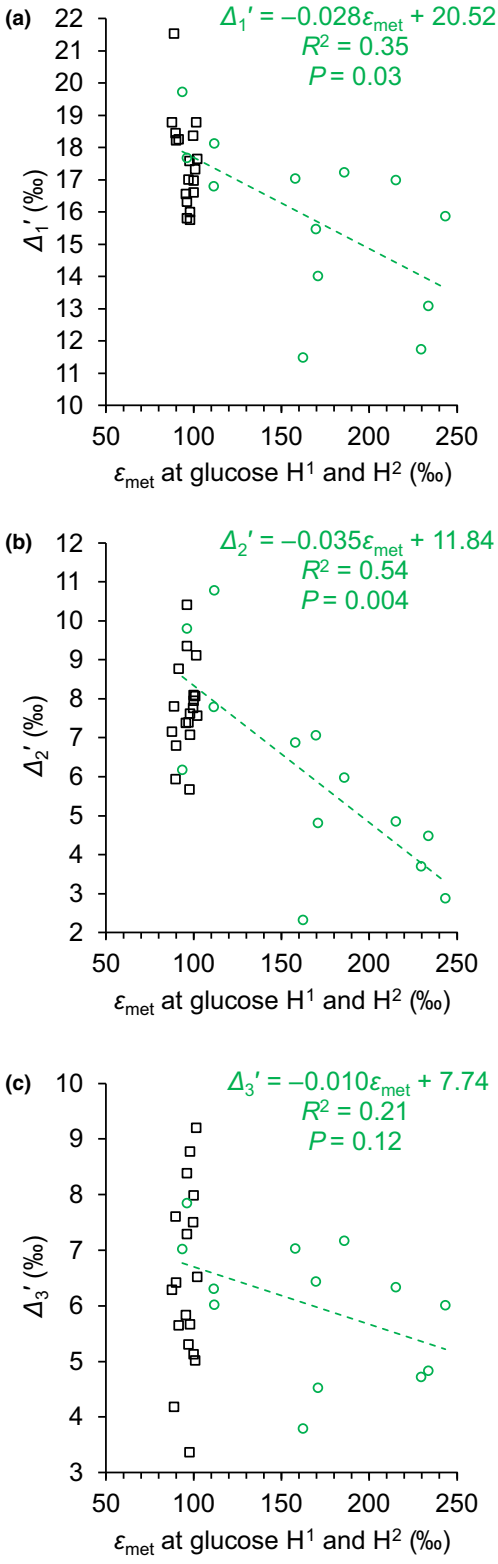

Fig. 3 Relationship between the average hydrogen isotope fractionation caused by metabolic processes at glucose H^1 and H^2 (ε_{met}) and ^{13}C discrimination at C-1, C-2, and C-3 ($\Delta_1{}'$, $\Delta_2{}'$, and $\Delta_3{}'$). Glucose was extracted across an annually resolved tree-ring series of *Pinus nigra* from the Vienna Basin (black squares, 1961–1980; green circles, 1983–1995). Dashed line, relationship between the hydrogen and carbon isotope data of the period 1983–1995.

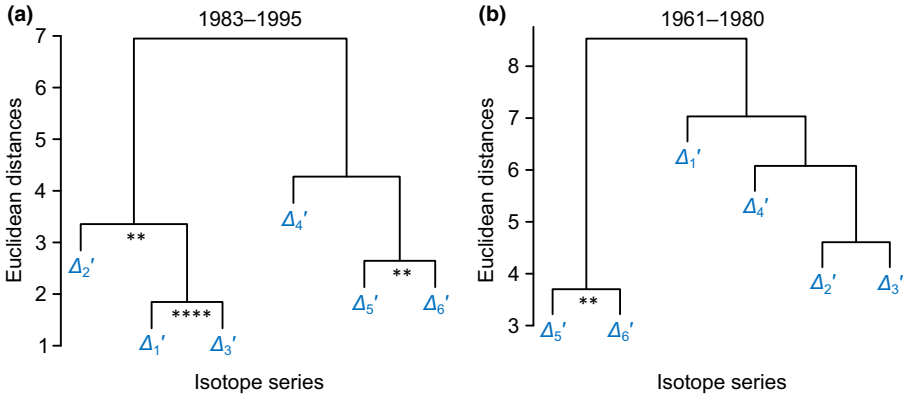

Fig. 4 Hierarchical clustering of Δ_i' series for the periods 1983–1995 (a) and 1961–1980 (b). Δ_i' denotes intramolecular ^{13}C discrimination in tree-ring glucose of *Pinus nigra* from the Vienna basin with *i* denoting individual glucose carbon positions. Significance of series correlation: **, $P \leq 0.01$; ****, $P \leq 10^{-4}$.

During the early period, Δ_1', Δ_2', and Δ_3' are not significantly correlated (Fig. 4b). Furthermore, isotope–environment models that work for the late period (Table 4 (M5–M7)) do not work for the early period (M8–M10). Compared with the late period, we found fewer and weaker isotope–climate correlations (Table 5).

Isotope–environment relationships at tree-ring glucose C-4 to C-6

As evident from our previously published hierarchical cluster analysis and Pearson's correlation analyses for the whole period, Δ_4', Δ_5', and Δ_6' share common variability, and Δ_5' and Δ_6' are significantly correlated (Fig. 1b; $r = 0.61$, $P < 0.001$, $n = 31$) (Wieloch *et al.*, 2018). This significant correlation holds for both the early and late period (Fig. 4). Furthermore, we did not find change points in the Δ_4', Δ_5', and Δ_6' series (Tables S1, S2). Therefore, we analysed isotope–environment relationships for the whole period. We found that Δ_5' and Δ_6' correlate with numerous climate parameters and periods but most significantly with *RAD* while significant Δ_4'-climate correlations are rare (Table 6). Models including April–September *RAD* and March–October *TMP* as cofactors capture 96% of the systematic variance in Δ_{5-6}', Δ_5', and Δ_6' of 73%, 66%, and 45%, respectively (Table 7 (M1–M3); Δ_{5-6}', $\text{adj}R^2 = 0.70$, $P = 10^{-7}$; Δ_5', $\text{adj}R^2 = 0.64$, $P = 10^{-6}$; Δ_6', $\text{adj}R^2 = 0.43$, $P < 0.001$; $n = 28$; Table S4). Based on *RAD* regression slopes (which are better constrained than *TMP* regression slopes), the ^{13}C discrimination at C-5 is *c.* 1.5 times larger than at C-6 (Table 7 (M2–M3)). The model works well for both the early and late period (Table 7 (M4–M5)). Furthermore, consistent with the weak association between Δ_4' and Δ_{5-6}' (Fig. 1b), the model works reasonably well for Δ_4', considering the relatively low systematic variance in Δ_4' of 38% (Tables 7 (M6), S4).

Discussion

Intramolecular carbon isotope analysis of tree-ring glucose yields information about metabolic variability and water status of both leaves and stems

We found evidence for processes affecting Δ_1' and Δ_3', which respond to *VPD* (Table 4 (M1, M3, M5)). Intriguingly, we also found evidence for processes simultaneously affecting ε_{met}, Δ_1', and Δ_2', which respond to *PRE* but not *VPD* (Tables 4 (M1, M2, M4, M6, M7, M11), S5). This sensitivity to different hydrological properties may be explained by the fact that stem capacitance can buffer stem water status against changes in *VPD* (McCulloh *et al.*, 2019), whereas leaf water status is tightly coupled to *VPD* (Grossiord *et al.*, 2020). Changes in *PRE* will affect soil water potential and hence both stem and leaf water status. Variability in leaf water status may be impacted more by *VPD* than by soil water status, which would explain why *VPD* is the best predictor of the intercorrelated processes affecting Δ_1' and Δ_3'. By contrast, *VPD*-insensitive processes affecting ε_{met}, Δ_1', and Δ_2' may reside in stems. Hence, we propose intramolecular carbon and hydrogen isotope analysis of tree-ring glucose yields information about metabolic variability and water status not only of leaves but also of stems. *PRE*-dependent systemic changes in enzyme expression can be considered as an alternative explanation.

Isotope fractionation mechanisms in leaves affecting tree-ring glucose C-1 to C-3

The Δ_{1-2}' and Δ_{1-3}' series exhibit change points in 1980; that is, their frequency distributions do not align with the properties of a single theoretical probability distribution (see the Results section; Tables S1, S2). Consequently, we investigated the early (1961–1980) and late period (1983–1995) separately. During the late period, Δ_1' and Δ_3' are significantly intercorrelated (Fig. 4a) and correlate negatively with *VPD* and positively with short-term *SPEI*, whereas Δ_2' lacks most of these correlations (Table 3). Furthermore, during the late period, growing season *VPD* accounts for a significant fraction of the systematic variance in Δ_1' and the entire systematic variance in Δ_3' but does not contribute significantly to explaining Δ_2' (Tables 4 (M1, M2, M5), S4). Hence, increasing *VPD* during 1983–1995 causes ^{13}C enrichments at tree-ring glucose C-1 and C-3 but not C-2. At C-1, the effect is about twice as large as at C-3 (Table 4 (M1 and M5)).

As discussed above, the *VPD*-dependent processes affecting Δ_1' and Δ_3' are likely located in leaves. Qualitatively, *VPD*-induced ^{13}C enrichments at C-1 and C-3 are consistent with the mechanisms of diffusion–rubisco fractionation (see the Introduction section). However, diffusion–rubisco fractionation affects all glucose carbon positions equally (Wieloch *et al.*, 2018). Hence,

Table 3 Significance of Pearson's correlations among Δ_1', Δ_2', and Δ_3' and climate series for the period 1983–1995 ($n = 13$).

	VPD			*PRE*			$SPEI_1$			$SPEI_3$			$SPEI_4$			$SPEI_6$			$SPEI_8$			$SPEI_{12}$			$SPEI_{16}$			$SPEI_{24}$			$SPEI_{36}$			$SPEI_{48}$			*TMP*			*SD*			*RAD*		
Period/Δ_i'	1	2	3	1	2	3	1	2	3	1	2	3	1	2	3	1	2	3	1	2	3	1	2	3	1	2	3	1	2	3	1	2	3	1	2	3	1	2	3	1	2	3	1	2	3
MAMJ	c	a	b		a		b		a	b		a	a																					a					a					
MAMJJ	c		b	a	a	a	b		b	b		a	b		a	a			a																									
MAMJJA	c		b	b	a	a	c		b	c		b	b		a	b			a															a									
MAMJJAS	c		b	b	b		b		a	c		b	c		a	b		a	b																				a				
MAMJJASO	c		b	a	a		b		a	c		a	c		a	b		a	b		a	a																a				
MAMJJASON	c		b	a	a		b		a	b		a	c		a	b		a	b		a	a															a		a				
AMJJ	c		c	a	a	a	a		b	b		b	b		b	b		a	a																a								
AMJJA	c		c	a	a	a	b		b	c		b	c		b	b		a	b		a													a		a						
AMJJAS	c		b	a	b	a	b		b	c		b	c		b	b		a	b		a	a																a				
AMJJASO	c		b	a	a		b		a	c		b	c		b	c		b	b		a	a		a												a		a				
AMJJASON	c		b	a	b		a		a	b		a	c		b	c		a	c		a	b		a													a		a				
MJJA	b		b	a			b		a	b		b	b		b	b		b	b		a	a		a												a		a				
MJJAS	b		b	b	a	a	b		a	c		b	c		b	c		b	b		a	b		a														a		a				
MJJASO	c		b	a			b		a	c		b	c		b	c		b	c		a	b		a														a		a				
MJJASON	c		b	a	a		a		a	b		a	c		b	c		b	c		a	b		a														a		a				
JJAS	b		b				a			b		b	b		b	c		b	b		a	b		a																				
JJASO	b		b							b		a	b		b	c		b	c		a	b		a																				
JJASON	b		a							b		a	b		a	b		b	c		b	b		a	a		a																
JASO	a		a							b		a	b		a	c		b	c		b	b		a	a		a							a									
JASON	a		a							a			b		a	b		b	c		b	b		a	a		a							a									
ASON	c		a										a			b		a	c		b	b		a	a		a							a				b					

Significance levels: a, ≤0.05 (light grey); b, ≤0.01 (medium grey); c, ≤0.001 (dark grey). Underline denotes negative correlation. Climate parameters: *PRE*, precipitation; *RAD*, global radiation; *SD*, sunshine duration; $SPEI_i$, standardised precipitation-evapotranspiration index of different periods ($i = 1, 3, 6, 8, 12, 16, 24, 36, 48$ months); *TMP*, air temperature; *VPD*, air vapour pressure deficit. Climate data were averaged for all ≥4-month periods of the growing season (March–November). Months were abbreviated by their initial letters. Δ_1', Δ_2', and Δ_3' denote intramolecular ^{13}C discrimination at glucose C-1, C-2, and C-3, respectively. Glucose was extracted across an annually resolved tree-ring series of *Pinus nigra*.

Table 4 Linear regression models of Δ_1', Δ_2', Δ_3', and ε_{met} as function of ε_{met}, growing season air vapour pressure deficit (*VPD*) and March–July precipitation (*PRE*).

M1: $\Delta_1' \sim \varepsilon_{met}$ + *VPD*, 1983–1995

$R^2 = 0.87$, adj$R^2 = 0.84$, $P < 10^{-4}$, $n = 13$

	Estimate	±SE	*P* ≤
Intercept	36.0	2.7	10^{-7}
ε_{met}	−0.0187	0.0057	0.01
VPD	−0.0295	0.0047	10^{-4}

M2: $\Delta_2' \sim \varepsilon_{met}$ + *VPD*, 1983–1995

$R^2 = 0.62$, adj$R^2 = 0.54$, $P < 0.008$, $n = 13$

	Estimate	±SE	*P* ≤
Intercept	17.6	4.5	0.003
ε_{met}	−0.0315	0.0097	0.009
VPD	−0.0111	0.0080	0.2

M3: $\Delta_3' \sim \varepsilon_{met}$ + *VPD*, 1983–1995

$R^2 = 0.64$, adj$R^2 = 0.57$, $P < 0.006$, $n = 13$

	Estimate	±SE	*P* ≤
Intercept	14.5	2.1	10^{-4}
ε_{met}	−0.00615	0.00449	0.2
VPD	−0.0129	0.0037	0.006

M4: $\Delta_2' \sim \varepsilon_{met}$, 1983–1995

$R^2 = 0.54$, adj$R^2 = 0.50$, $P < 0.004$, $n = 13$

	Estimate	±SE	*P* ≤
Intercept	11.8	1.7	10^{-4}
ε_{met}	−0.0351	0.0097	0.004

M5: $\Delta_3' \sim$ *VPD*, 1983–1995

$R^2 = 0.57$, adj$R^2 = 0.53$, $P < 0.003$, $n = 13$

	Estimate	±SE	*P* ≤
Intercept	14.3	2.2	10^{-4}
VPD	−0.0143	0.0037	0.003

M6: $\Delta_1' \sim$ *PRE* + *VPD*, 1983–1995

$R^2 = 0.82$, adj$R^2 = 0.79$, $P < 0.001$, $n = 13$

	Estimate	±SE	*P* ≤
Intercept	27.8	4.4	10^{-4}
PRE	0.0146	0.0061	0.04
VPD	−0.0280	0.0058	0.001

M7: $\Delta_2' \sim$ *PRE*, 1983–1995

$R^2 = 0.43$, adj$R^2 = 0.37$, $P < 0.02$, $n = 13$

	Estimate	±SE	*P* ≤
Intercept	−1.84	2.79	0.52
PRE	0.0274	0.0096	0.016

M8: $\Delta_3' \sim$ *VPD*, 1961–1980

$R^2 = 0.13$, adj$R^2 = 0.07$, $P = 0.15$, $n = 18$

	Estimate	±SE	*P* ≤
Intercept	12.3	3.8	0.006
VPD	−0.0112	0.0074	0.15

M9: $\Delta_1' \sim$ *PRE* + *VPD*, 1961–1980

$R^2 = 0.07$, adj$R^2 = 0$, $P > 0.55$, $n = 18$

	Estimate	±SE	*P* ≤
Intercept	18.6	4.8	0.002
PRE	0.00273	0.00407	0.51
VPD	−0.00357	0.00781	0.65

M10: $\Delta_2' \sim$ *PRE*, 1961–1980

$R^2 = 0.05$, adj$R^2 = 0$, $P = 0.35$, $n = 18$

	Estimate	±SE	*P* ≤
Intercept	6.92	0.93	10^{-5}
PRE	0.00276	0.00286	0.35

M11: $\varepsilon_{met} \sim$ *PRE* + *VPD*, 1983–1995

$R^2 = 0.71$, adj$R^2 = 0.66$, $P < 0.002$, $n = 13$

	Estimate	±SE	*P* ≤
Intercept	437	118	0.004
PRE	−0.777	0.164	0.001
VPD	−0.082	0.155	0.61

ε_{met}, Δ_1', Δ_2', and Δ_3' denote hydrogen isotope fractionation caused by metabolic processes at glucose H^1 and H^2, and carbon isotope discrimination at glucose C-1, C-2, and C-3, respectively. Glucose was extracted across an annually resolved tree-ring series of *Pinus nigra* from the Vienna Basin.

the unequal *VPD* response of Δ_1', Δ_2', and Δ_3' points to post-rubisco fractionations. In the following, we assume Δ_3' variation derives entirely from diffusion–rubisco fractionation and argue *VPD*-dependent isotope fractionation at PGI and G6PD in leaf chloroplasts and the cytosol may exert additional control over Δ_1' and Δ_2' variability. Generally, variability in PGI fractionation depends on three biochemical properties: (1) the equilibrium status of the PGI reaction, and relative flux of the PGI reactants (2) F6P and (3) G6P into competing metabolic pathways (Figs 2, 5):

(**1**) PGI reversibly converts F6P into G6P (Fig. 5a). Under non-stress conditions, the PGI reaction in chloroplasts is strongly

Table 5 Significance of Pearson's correlations among Δ_1', Δ_2', and Δ_3' and climate series for the period 1961–1980 ($n = 18$).

	VPD			*PRE*			$SPEI_1$			$SPEI_3$			$SPEI_4$			$SPEI_6$			$SPEI_8$			$SPEI_{12}$			$SPEI_{16}$			$SPEI_{24}$			$SPEI_{36}$			$SPEI_{48}$			*TMP*			*SD*			*RAD*		
Period/Δ_i'	1	2	3	1	2	3	1	2	3	1	2	3	1	2	3	1	2	3	1	2	3	1	2	3	1	2	3	1	2	3	1	2	3	1	2	3	1	2	3	1	2	3
MAMJ	a						a			a			a									a			a												a			a		
MAMJJ										a												a			a																	
MAMJJA																						a			a																	
MAMJJAS						a																a			b			a													
MAMJJASO							a															a			b			a													
MAMJJASON																						a			b			a													
AMJJ										a			a									a			b																	
AMJJA						a																a			b																	
AMJJAS						b			a													a			b			a													
AMJJASO						a																a			b			a													
AMJJASON						a																a			b			a													
MJJA					a	a																a			b			a													
MJJAS					a	b			a													a			b			a													
MJJASO						a																			b			a													
MJJASON						a																			b			a													
JJAS					a	b			a																b			a			a										
JJASO																									b			a			a										
JJASON																									b			a			a										
JASO			a																						b			a			a										
JASON								a																	b			a			a										
ASON			a																						b			a			a										

Significance levels: a, ≤0.05 (light grey); b, ≤0.01 (medium grey). Underline denotes negative correlation. Climate parameters: *PRE*, precipitation; *RAD*, global radiation; *SD*, sunshine duration; $SPEI_i$, standardised precipitation-evapotranspiration index of different periods ($i = 1, 3, 6, 8, 12, 16, 24, 36, 48$ months); *TMP*, air temperature; *VPD*, air vapour pressure deficit. Climate data were averaged for all ≥ 4-month periods of the growing season (March–November). Months were abbreviated by their initial letters. Δ_1', Δ_2', and Δ_3' denote intramolecular ^{13}C discrimination at glucose C-1, C-2, and C-3, respectively. Glucose was extracted across an annually resolved tree-ring series of *Pinus nigra*.

Table 6 Significance of Pearson's correlations among Δ_4', Δ_5', and Δ_6' and climate series for the period 1961–1995 ($n = 31$).

	VPD			PRE			*SPEI*$_1$			*SPEI*$_3$			*SPEI*$_4$			*SPEI*$_6$			SPEI$_8$			SPEI$_{12}$			*SPEI*$_{16}$			*SPEI*$_{24}$			*SPEI*$_{36}$			*SPEI*$_{48}$			TMP			SD			*RAD*		
Period/Δ_i'	4	5	6	4	5	6	4	5	6	4	5	6	4	5	6	4	5	6	4	5	6	4	5	6	4	5	6	4	5	6	4	5	6	4	5	6	4	5	6	4	5	6	4	5	6
MAMJ																						a			a														b			b		
MAMJJ		a			a			a			a														a													b			b		a
MAMJJA		a			a			a			a			a																								b			b		b
MAMJJAS		a									a			a			a																					b			b		b
MAMJJASO											a			a			a			a																		a			b		b
MAMJJASON		a												a			a			a																		a			b		b
AMJJ		b	a		b			c	a		b			a										a												a			c			c		a
AMJJA		b	a		b			b	a		b			b			a			a																a		a	c		a	c		b
AMJJAS		a	a		a			b	a		b			b			a			a																		a	c		a	c		c
AMJJASO		a	a		a			b	a		a			b			b			a																		a	b			c		c
AMJJASON		a	a					a	a		a			a			a			a																		a	b			c		c
MJJA		b	a	a	a			b	a		c	a		b			b			a																		a	b		a	c		b
MJJAS		a	a	a	a			b	a		b	a		b	a		b			a																		a	b		a	b		c
MJJASO		a	a	a	a			b	a		b	a		b	a		b	a		a			a															a		b			b		c
MJJASON		a	a					a	a		a	a		b	a		b	a		b			a														a	b		a			b		c
JJAS		a	a								b	a		b	a		b			a			a															b			a		a		c
JJASO			a								b	a		b	a		b	a		a			a															a						c
JJASON		a	a								a	a		a	a		b	a		b			a															a			a			c
JASO			a								a	a		b	a		b	a		b			a												a									b
JASON			a									a		a	a		b	a		b	a		a															a							b
ASON					a												b	a		a			a																						b

Significance levels: a, ≤0.05 (light grey); b, ≤0.01 (medium grey); c, ≤0.001 (dark grey). Underline denotes negative correlation. Climate parameters: *PRE*, precipitation; *RAD*, global radiation; *SD*, sunshine duration; *SPEI*$_i$, standardised precipitation-evapotranspiration index of different periods ($i = 1, 3, 6, 8, 12, 16, 24, 36, 48$ months); *TMP*, air temperature; *VPD*, air vapour pressure deficit. Climate data were averaged for all ≥4-month periods of the growing season (March–November). Months were abbreviated by their initial letters. Δ_4', Δ_5', and Δ_6' denote intramolecular ^{13}C discrimination at glucose C-4, C-5, and C-6, respectively. Glucose was extracted across an annually resolved tree-ring series of *Pinus nigra*.

displaced from equilibrium on the side of F6P (Dietz, 1985; Gerhardt *et al.*, 1987; Kruckeberg *et al.*, 1989; Schleucher *et al.*, 1999; Wieloch, 2022; Wieloch *et al.*, 2022a). With decreasing p_i, however, the reaction moves towards equilibrium (Dietz, 1985; Wieloch *et al.*, 2022a). This shift is accompanied by ^{13}C increases at C-1 and C-2 of G6P (Table 2), which will be transmitted to downstream derivatives such as starch and tree-ring glucose (Wieloch *et al.*, 2018). In isohydric species such as *P. nigra*, p_i decreases with drought due to stomatal closure (McDowell *et al.*, 2008). Here, we found stronger *VPD*-induced ^{13}C increases at tree-ring glucose C-1 than at C-3. This is consistent with the PGI-related isotope shift expected at C-1. However, the apparent absence of the diffusion–rubisco signal from C-2 contrasts with the expected isotope shift. That said, in *Phaseolus vulgaris*, the ratio of leaf sucrose-to-starch carbon partitioning was shown to increase steeply with decreasing p_i (Sharkey *et al.*, 1985). Hence, the relative contribution of chloroplastic G6P and its isotope composition to downstream metabolism may decrease with increasing *VPD*, reducing the influence of the mechanism described on Δ_1' and Δ_2' variation.

(**2**) In natural systems, leaf night-time respiration is increased under drought (Fig. 5b; Schmiege *et al.*, 2023). Furthermore, in the dark, the cytosolic PGI reaction was found to be near equilibrium (Gerhardt *et al.*, 1987). Consequently, F6P would be ^{13}C depleted at C-1 but ^{13}C enriched at C-2 relative to the corresponding G6P positions (Table 2). Increasing relative F6P flux into mitochondrial respiration would then result in ^{13}C increases at C-1 and ^{13}C decreases at C-2 of G6P and downstream derivatives. Thus, this mechanism is consistent with both observations, stronger *VPD*-induced ^{13}C increases at tree-ring glucose C-1 compared with C-3, and the apparent absence of the diffusion–rubisco signal from C-2.

(**3**) While carbon assimilation commonly decreases with drought (McDowell *et al.*, 2008), the activity of leaf-cytosolic G6PD increases (Fig. 5c; Landi *et al.*, 2016). This can be expected to result in increasing relative G6P flux into the OPPP. While some authors reported that the cytosolic PGI reaction in illuminated leaves is in equilibrium (Gerhardt *et al.*, 1987), others found displacements from equilibrium (Leidreiter *et al.*, 1995; Schleucher *et al.*, 1999; Szecowka *et al.*, 2013). Hence, PGI-related isotope shifts in tree-ring glucose resulting from G6P flux into the leaf-cytosolic OPPP are hard to predict (Table 2). By contrast, the unidirectional conversion of G6P to 6-phosphogluconolactone catalysed by G6PD proceeds faster with ^{12}C-1 than ^{13}C-1 G6P ($k_{^{12}C}/k_{^{13}C} = 1.0165$) (Hermes *et al.*, 1982). Hence, increasing relative flux through the leaf-cytosolic OPPP may contribute to the stronger *VPD*-induced ^{13}C increases at tree-ring glucose C-1 compared with C-3.

Aside from these mechanisms, there are others that might introduce Δ_1' and Δ_2' variation. For instance, we recently reported evidence consistent with increasing relative flux through the chloroplastic OPPP in response to decreasing p_i under illumination (Fig. 5a; Wieloch *et al.*, 2022a, 2023). Furthermore, under illumination, chloroplastic F6P is used for both RuBP regeneration and starch biosynthesis (Fig. 5a). Increasing *VPD*

Table 7 Linear regression models of Δ_4', Δ_5', and Δ_6' as function of April–September global radiation (*RAD*), and March–October air temperature (*TMP*).

M1: $\Delta_{5-6}' \sim$ *RAD* + *TMP*, 1964–1995

$R^2 = 0.72$, adj$R^2 = 0.70$, $P = 10^{-7}$, $n = 28$

	Estimate	±SE	$P \leq$
Intercept	26.0	3.1	10^{-8}
RAD	−0.00843	0.00105	10^{-7}
TMP	1.35	0.29	10^{-4}

M2: $\Delta_5' \sim$ *RAD* + *TMP*, 1964–1995

$R^2 = 0.66$, adj$R^2 = 0.64$, $P = 10^{-6}$, $n = 28$

	Estimate	±SE	$P \leq$
Intercept	24.8	4.3	10^{-5}
RAD	−0.0103	0.0015	10^{-6}
TMP	1.81	0.40	10^{-4}

M3: $\Delta_6' \sim$ *RAD* + *TMP*, 1964–1995

$R^2 = 0.47$, adj$R^2 = 0.43$, $P < 0.001$, $n = 28$

	Estimate	±SE	$P \leq$
Intercept	27.3	4.2	10^{-6}
RAD	−0.00658	0.00144	10^{-4}
TMP	0.876	0.393	0.04

M4: $\Delta_{5-6}' \sim$ *RAD* + *TMP*, 1964–1980

$R^2 = 0.69$, adj$R^2 = 0.63$, $P < 0.001$, $n = 15$

	Estimate	±SE	$P \leq$
Intercept	31.2	6.7	0.001
RAD	−0.00906	0.00177	0.001
TMP	1.11	0.47	0.04

M5: $\Delta_{5-6}' \sim$ *RAD* + *TMP*, 1983–1995

$R^2 = 0.82$, adj$R^2 = 0.79$, $P < 0.001$, $n = 13$

	Estimate	±SE	$P \leq$
Intercept	29.1	4.5	10^{-4}
RAD	−0.00875	0.00132	10^{-4}
TMP	1.22	0.40	0.01

M6: $\Delta_4' \sim$ *RAD* + *TMP*, 1964–1995

$R^2 = 0.15$, adj$R^2 = 0.09$, $P = 0.12$, $n = 28$

	Estimate	±SE	$P \leq$
Intercept	8.33	4.73	0.09
RAD	−0.00266	0.00160	0.11
TMP	0.931	0.439	0.04

Δ_4', Δ_5', and Δ_6' denote carbon isotope discrimination at glucose C-4, C-5, and C-6, respectively. Glucose was extracted across an annually resolved tree-ring series of *Pinus nigra* from the Vienna Basin.

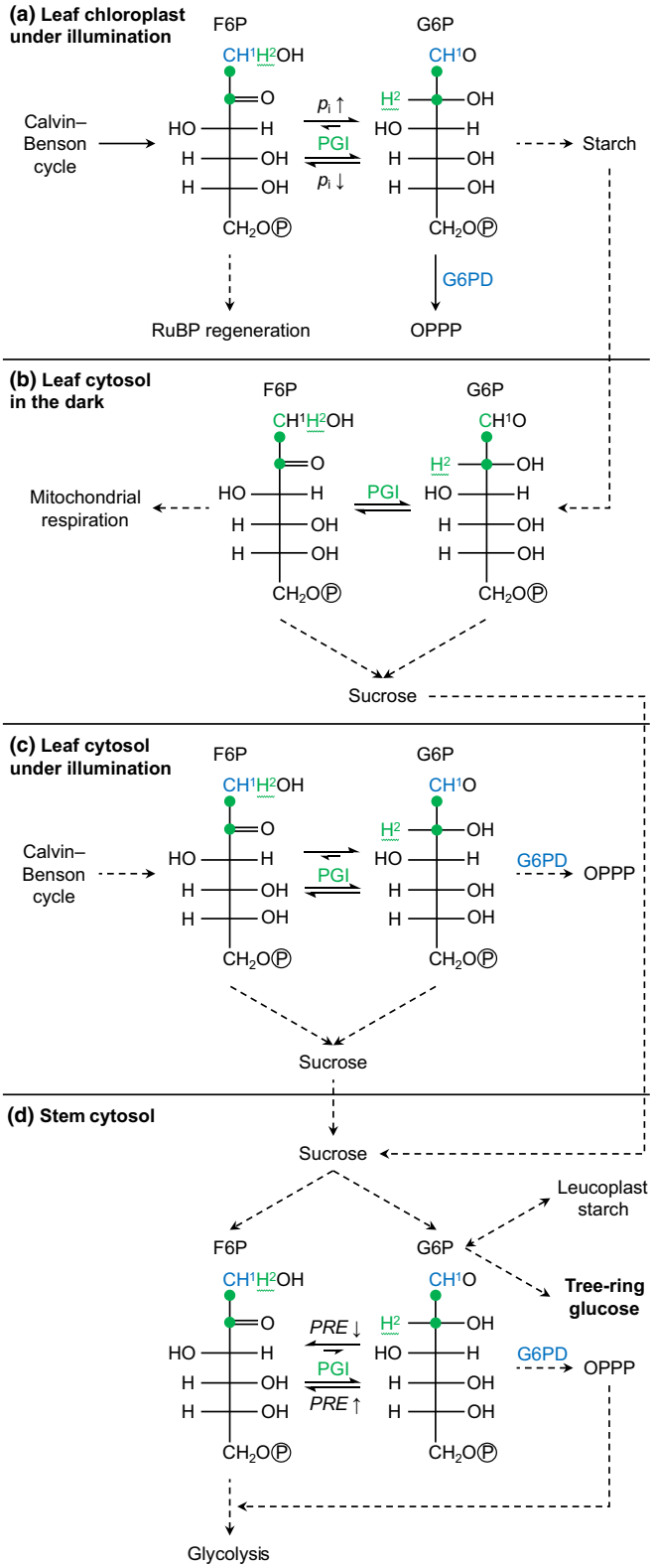

Fig. 5 Processes invoked to explain isotope fractionation at tree-ring glucose HC-1 and HC-2: (a) in leaf chloroplasts under illumination, (b) in the leaf cytosol in the dark, (c) in the leaf cytosol under illumination, and (d) in the stem cytosol. F6P and G6P carbon atoms 1–6 occur in sequentially order from top to bottom. Atom positions affected by G6PD and PGI fractionation are given in blue and green, respectively. In some cases, carbon position 1 is given both as blue letter and green dot to indicate fractionation at both enzymes. Dashed arrows indicate that intermediate reactions are not shown. Wavy lines indicate fractional introduction of hydrogen from water by the PGI reaction. Note that G6PD in stem leucoplasts may additionally contribute to isotope fractionation at tree-ring glucose C-1 and H^1. F6P, fructose 6-phosphate; G6P, glucose 6-phosphate; G6PD, G6P dehydrogenase; OPPP, oxidative pentose phosphate pathway; PGI, phosphoglucose isomerase; p_i, intercellular CO_2 partial pressure; *PRE*; precipitation; RuBP, ribulose 1,5-bisphosphate.

promotes photorespiration resulting in increasing RuBP regeneration relative to carbon export from the Calvin–Benson cycle into sinks such as starch.

The mechanisms described above should also introduce hydrogen isotope signals because of the hydrogen isotope effects of G6PD affecting G6P H^1 (Hermes *et al.*, 1982) and PGI affecting G6P H^2 (Table 2; Fig. 5). However, growing season *VPD* neither correlates with ε_{met} pertaining to tree-ring glucose H^1 nor H^2 (Tables S5, S6). Hence, either G6PD and PGI are not the sources of *VPD*-dependent carbon isotope fractionation in Δ_1' (and Δ_2'), or the corresponding hydrogen isotope signals were washed out after introduction. Washout at H^1 may occur during equilibration of F6P with mannose 6-phosphate by phosphomannose isomerase (cf. Topper, 1957). Similarly, complete washout at H^2 may occur when the leaf-cytosolic PGI reaction is in equilibrium (Notes S3). Previously, this latter process was invoked (among others) to explain why a whole-molecule deuterium depletion observed in leaf starch was not transmitted to nocturnal sucrose (see the Introduction section; Wacker, 2022). As each conversion by PGI was found to be associated with a 0–50% probability for hydrogen exchange with the medium (Noltmann, 1972), partial washout of existing hydrogen isotope signals may also occur under nonequilibrium conditions (Notes S3).

In the mechanisms described above, we assumed diffusion–rubisco fractionation contributes to *VPD*-dependent Δ_i' variation. However, diffusion–rubisco fractionation affects all glucose carbon positions equally (Wieloch *et al.*, 2018). Since merely two of six glucose carbon positions carry *VPD*-dependent isotope variation, the question arises of whether the diffusion–rubisco signal was already below the detection level on introduction. If this were the case, then *VPD*-dependent Δ_1' and Δ_3' variation would originate entirely from post-rubisco processes. Furthermore, post-rubisco processes that were previously invoked to explain the absence of the diffusion–rubisco signal from C-4, C-5, and C-6 (see the Introduction section) would not occur.

Isotope fractionation mechanisms in stems affecting tree-ring glucose HC-1 and HC-2

Previously, we found a change point in ε_{met} in 1980 (Wieloch *et al.*, 2022b). Here, we found the same change point in Δ_{1-2}' (see the Results section). Consistent with this, Δ_1' and Δ_2' data of 1983–1995 exhibit a significantly lower average value and a

significantly larger variance than those of 1961–1980 (Tables S1, S2). Furthermore, $\Delta_1{}'$ and $\Delta_2{}'$ are significantly correlated during the late (Fig. 4a) but not the early period (Fig. 4b), and ε_{met} accounts for a significant fraction of the variance of both $\Delta_1{}'$ and $\Delta_2{}'$ during the late period (Table 4 (M1, M4); Fig. 3a,b). In $\Delta_2{}'$, the ε_{met} effect is about twice as large as in $\Delta_1{}'$. Processes affecting ε_{met}, $\Delta_1{}'$, and $\Delta_2{}'$ simultaneously respond to *PRE* but not *VPD* (Tables 4 (M1, M2, M4, M6, M7, M11), S5). $\Delta_1{}'$ and $\Delta_2{}'$ respond to March–July *PRE* during the late but not the early period (Table 4 (M9–M10)). Previously, we reported evidence suggesting the groundwater table before 1980 was high enough to prevent metabolic changes causing ε_{met} variation (Wieloch *et al.*, 2022b). By extension, this should also explain the properties of $\Delta_1{}'$ and $\Delta_2{}'$ listed above. That is, since the trees had access to groundwater during the early period, metabolic shifts that can cause intercorrelated variation in ε_{met}, $\Delta_1{}'$, and $\Delta_2{}'$ were not induced.

Processes causing intercorrelated variation in ε_{met}, $\Delta_1{}'$, and $\Delta_2{}'$ are probably located in the stem (see the first section of the Discussion section). The ε_{met} signal is present at glucose H^1 and, considerably more strongly, at H^2 (range: 64‰ and 240‰, respectively; 1983–1995). In the biochemical pathway leading to tree-ring cellulose, PGI is the last enzyme acting on precursors of glucose H^2 (Figs 2, 5d). With each conversion by PGI, there is a probability for hydrogen exchange with the medium of 0–50% (Noltmann, 1972). Thus, if we assume *P. nigra* stem PGI exchanges hydrogen with the medium as does spinach leaf PGI (Fedtke, 1969) and the reaction is in equilibrium, then any deuterium signal at G6P H^2 will be washed out. Among all H-C positions of tree-ring glucose, the deuterium abundance at H^2 is neither exceptionally high nor low during 1961–1980, whereas it is exceptionally high (and exceptionally variable) during 1983–1995 (Fig. 6). This indicates that the PGI reaction was close to or in equilibrium during 1961–1980 but displaced from equilibrium on the side of G6P during 1983–1995 (Table 2). Additionally, shifts of the PGI reaction away from equilibrium towards the side of G6P should cause ^{13}C enrichment at G6P C-1 and C-2 ($\Delta_1{}'$ and $\Delta_2{}'$ decreases), and $\Delta_2{}'$ should decrease three times more than $\Delta_1{}'$ (Table 2). Consistent with this, we found negative relationships between ε_{met} and $\Delta_1{}'$, as well as $\Delta_2{}'$ (Table 4 (M1 and M4)). However, $\Delta_2{}'$ decreases only 1.88 times more than $\Delta_1{}'$, but this best estimate is associated with a relatively large error (SE interval: 1.04–3.45). That said, the offset from 3 is likely explained by increasing relative flux through the OPPP accompanying the putative PGI reaction shift (Figs 2, 5d). This is because G6P to 6-phosphogluconolactone conversion by G6PD exhibit ^{13}C and D isotope effects ($k_{12C}/k_{13C} = 1.0165$, $k_H/k_D = 2.97$) (Hermes *et al.*, 1982). Hence, increasing relative OPPP flux causes ^{13}C enrichment at G6P C-1 ($\Delta_1{}'$ decreases) and deuterium enrichment at G6P H^1. This is consistent with both the apparently decreased PGI effects ratio (1.88 instead of 3) and, more importantly, ε_{met} increases at glucose H^1 of up to 64‰ during 1983–1995 (Fig. 6).

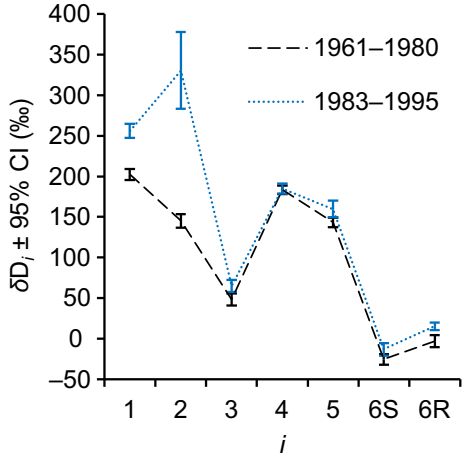

Fig. 6 Average intramolecular δD_i patterns of the periods 1961–1980 and 1983–1995 (black and blue, respectively). The data were acquired for tree-ringglucose of *Pinus nigra* laid down at a site in the Vienna basin. $\delta D_i = D_i / (\Sigma D_{ME}/6)$-1 where D_i denotes the deuterium abundance at glucose hydrogen position *i* and $\Sigma D_{ME}/6$ denotes the average deuterium abundance of the six methyl-group hydrogens of the glucose derivative used for NMRS measurements. Error bars represent 95% confidence intervals. The figure shows discrete data. Dashed and dotted lines were added to guide the eye. Modified figure from Wieloch *et al*. (2022b).

Sucrose translocated from leaves can be split into UDP-glucose and fructose via sucrose synthase or glucose and fructose via invertase (Fig. 2). UDP-glucose entering tree-ring cellulose biosynthesis directly via sucrose synthase is protected from isotope fractionation by PGI and G6PD. However, in stems of juvenile *Quercus petraea* and *Picea abies*, at least 79% and 43% of the precursors of tree-ring glucose went through PGI catalysis, respectively (Augusti *et al.*, 2006). Theoretically, shifts of the PGI reaction away from equilibrium towards the side of G6P can cause ε_{met} increases at glucose H^2 of up to 611‰ (Notes S3, hydrogen exchange with the medium not considered). With 43% and 79% of all precursors of tree-ring glucose undergoing PGI catalysis, ε_{met} increases at glucose H^2 of up to 263‰ and 483‰ are possible, respectively. Thus, the PGI-related fractionation mechanism proposed here can potentially cause previously reported ε_{met} increases at glucose H^2 of up to 240‰ (Wieloch *et al.*, 2022b). Shifts in sucrose cleavage by sucrose synthase vs invertase may exert additional control over the ε_{met} signal at glucose H^2.

Based on results and interpretations presented above, decreasing stem water content is associated with both increasing OPPP flux and a shift of the PGI reaction away from equilibrium towards the side of G6P corresponding to low relative F6P concentration (Fig. 5d). We propose these concerted shifts may ensure redox homeostasis and balanced substrate supply to glycolysis as follows. In heterotrophic tissue, NADPH from the OPPP is believed to be central for maintaining redox homeostasis (Fig. 2; Stincone *et al.*, 2015). Flux through the OPPP is regulated at G6PD. Heterotrophic G6PD activity reportedly increases with drought (Liu *et al.*, 2013; Wang *et al.*, 2016, 2020), oxidative load (Wang *et al.*, 2016, 2020; Li *et al.*, 2020), NADPH demand (Wendt *et al.*, 2000; Esposito *et al.*, 2001; Castiglia *et al.*, 2015), and abscisic acid concentration (Cardi *et al.*, 2011; Wang *et al.*, 2016). Decreasing stem water content may cause increasing OPPP flux via increasing abscisic acid concentration (Brunetti *et al.*, 2020), and possibly increasing

oxidative load increasing the demand for NADPH. In turn, increasing OPPP flux results in increasing supply of pentose phosphates, which may feed into glycolysis via the reductive part of the pentose phosphate pathway (Figs 2, 5d). This would reduce the demand for glycolytic substrates supplied via PGI. The shift of the PGI reaction away from equilibrium towards the side of G6P may reflect this decreased demand and result from PGI downregulation by intermediates of the pentose phosphate pathway such as erythrose 4-phosphate, ribulose 5-phosphate, and 6-phosphogluconate (Parr, 1956; Grazi *et al.*, 1960; Salas *et al.*, 1965). Furthermore, relative changes in G6P-to-F6P supply vs consumption may contribute to the shift of the PGI reaction. For instance, while starch storage consumes G6P, remobilisation supplies G6P (Noronha *et al.*, 2018). Under drought, the storage-to-remobilisation balance may tilt towards remobilisation (Mitchell *et al.*, 2013; Thalmann & Santelia, 2017; Tsamir-Rimon *et al.*, 2021). Consequently, the PGI reaction may move towards the side of G6P. Similarly, we previously reported below-average tree-ring widths for years in which the PGI reaction is on the side of G6P (Wieloch *et al.*, 2022b). Hence, in these years, G6P consumption by growth may have been reduced while F6P consumption by downstream metabolism may have been maintained.

1961–1980: A period of homeostasis with respect to processes affecting Δ_1', Δ_2', Δ_3', and ε_{met}

During 1961–1980, Δ_1', Δ_2', and Δ_3' are not significantly correlated which contrasts with the period 1983–1995 (Fig. 4a,b). Similarly, relationships of Δ_1' and Δ_3' with *VPD* and Δ_1' and Δ_2' with *PRE* observed during the late period are largely absent during the early period (Tables 3–5) even though there is no difference in the magnitude of *VPD* and *PRE* variability between these periods (Fig. S1). Like Δ_{1-2}' and Δ_{1-3}', ε_{met} exhibits a change point in 1980 and responds to *PRE* after but not before 1980 (Wieloch *et al.*, 2022b). This shift in ε_{met} sensitivity was attributed to long-term drought, which intensified over the study period and proposedly lead to a groundwater depletion below a critical level in 1980 (Wieloch *et al.*, 2022b). By extension, this groundwater depletion might also explain the insensitivity of Δ_1' and Δ_3' to *VPD* and Δ_1' and Δ_2' to *PRE* during 1961–1980 and their sensitivity from 1983 onwards. Thus, while the trees had access to groundwater, leaf- and stem-level processes affecting Δ_1', Δ_2', Δ_3' and ε_{met} could apparently maintain homeostasis despite changing atmospheric conditions.

Isotope fractionation mechanisms in leaves affecting tree-ring glucose C-5 and C-6

No change points were detected in Δ_5' and Δ_6' (see the Results section; Tables S1, S2). Furthermore, Δ_5' and Δ_6' remain significantly correlated across the entire study period (Figs 1b, 4a,b), and *RAD* is the most influential environmental cofactor (Table 6). Models including *RAD* and *TMP* as cofactors capture most of the systematic variance in Δ_{5-6}', Δ_5', and Δ_6' (Tables 7 (M1–M3), S4). These relationships hold for both the early and late study period (Table 7 (M4–M5)) with Δ_5' effects being *c.* 1.5-fold larger than Δ_6' effects (M2 vs M3, SE interval: 1.1–2.28).

Previously, we reported a negative relationship between tree-ring glucose Δ_{5-6}' and reconstructed tropospheric O_3 concentration (see the Introduction section; Wieloch *et al.*, 2022c). Light stimulates tropospheric O_3 formation (Lu *et al.*, 2019). This may explain the negative relationship between tree-ring glucose Δ_{5-6}' and *RAD* reported here (Table 7 (M1–M3)). Furthermore, we previously explained the absence of the diffusion–rubisco signal from glucose C-5 and C-6 (*inter alia*) by interaction between photorespiration and the TCAC (see the Introduction section; Wieloch *et al.*, 2022c). As *TMP* increases, photorespiration increases more than photosynthesis (Long, 1991). This may result in decreasing flux of PEP into the TCAC (see the Introduction section) and explain the positive relationship between tree-ring glucose Δ_{5-6}' and *TMP* reported here (Table 7 (M1–M3)).

Isotope fractionation mechanisms in leaves affecting tree-ring glucose C-4

As for Δ_5' and Δ_6', no change point was detected in Δ_4' (see the Results section; Tables S1, S2). Considering the entire study period, Δ_4' is weakly associated with Δ_{5-6}' (Fig. 1b). Consistent with this, the Δ_{5-6}'-climate model works reasonably well for Δ_4' considering the relatively low systematic variance in Δ_4' of 38% (Tables 7 (M1 and M6), S4). Introduction of the Δ_4' and Δ_{5-6}' signals proposedly involves leaf-level consumption of PGA and PEP by downstream metabolism, respectively (Wieloch *et al.*, 2021, 2022c). Since PGA is a precursor of PEP (Fig. 2), our previously proposed theories of signal introduction are in line with the observation that Δ_4', Δ_5' and Δ_6' are associated and respond to the same environmental parameters.

Conclusions and future directions

Dual-isotope-environment analysis was used to deconvolute isotope signals and provide several new insights into plant isotope fractionation. First, the diffusion–rubisco signal was previously shown to be absent from tree-ring glucose C-4 to C-6 (Wieloch *et al.*, 2021, 2022c) but believed to be present at C-1 to C-3 (Wieloch *et al.*, 2018). Here, this signal was found to also be absent from C-2. Second, isotope fractionation beyond leaves is commonly considered to be constant for any given species (Roden *et al.*, 2000; Gagen *et al.*, 2022). However, our results suggest a significant part of the carbon and hydrogen isotope variation in tree-ring glucose originates in stems from processes affecting Δ_1', Δ_2', and ε_{met} simultaneously. Third, *VPD* affects Δ_1' and Δ_3' and *PRE* affects Δ_1', Δ_2', and ε_{met} (Table 4). These relationships proposedly reflect water content variability in leaves and stems, respectively. They apply to the late but not the early study period consistent with the finding of a change point in both the ε_{met} (Wieloch *et al.*, 2022b) and Δ_{1-3}' series. This change point proposedly marks the crossing of a physiologically relevant groundwater threshold (Wieloch *et al.*, 2022b). Additionally, we reported Δ_{5-6}' relationships with *RAD* and

TMP, which apply to the entire study period (Table 4). These latter relationships are consistent with previously proposed isotope fractionation mechanisms (Wieloch *et al.*, 2022c). By contrast, we here revised and expanded our previous theory on the mechanisms introducing $\Delta_1{}'$, $\Delta_2{}'$, $\Delta_3{}'$, and ε_{met} variability. Given the multitude of isotope-environment relationships (including change point responses), intramolecular carbon isotope analysis has a remarkable potential for reconstructions of environmental conditions (*VPD*, *PRE*, *RAD*, *TMP*, soil moisture, groundwater thresholds, tropospheric O_3 concentration), tissue water content (leaf, stem), metabolic flux variability (various processes), and ecophysiological properties such as intrinsic water-use efficiency across space and time. Complementing hydrogen isotope analysis is expected to significantly enhance these capabilities.

Understanding isotope fractionation mechanisms is central for retrospective studies of plant physiology and climate based on tree-ring isotope data, and there is considerable room for improvement as shown above. Research in several largely unexploited areas is needed to make progress. First, there is a basic need for more *in vitro* data on intramolecular isotope effects of enzyme reactions including the reactions catalysed by triosephosphate isomerase, transketolase, PEPC, PK, and DAHPS. Second, intramolecular isotope analyses of leaf metabolites including starch and sucrose from both controlled and natural environments are needed to generate a baseline for mechanistic studies of isotope fractionation along the pathway from leaves to wood. Additionally, intramolecular isotope analysis of metabolites from wood slices acclimated to different ambient conditions (e.g. wet vs dry, varying sucrose supply) will be insightful. Third, combined analysis of intramolecular ^{13}C and deuterium data can help to separate isotope signals. Fourth, genetic modification of key enzymes may help to test proposed isotope fractionation mechanisms *in vivo*. Fifth, intramolecular isotope fractionation affecting tree-ring glucose is complex. Software programs such as QIRN enable the convenient simulation of natural isotope abundances in complex metabolic networks (Mueller *et al.*, 2022). If expanded, these programs may help to extract metabolic information from intramolecular tree-ring isotope data. This would require routines enabling control of relative flux at metabolic branchpoints by optimising regressions between (1) relative branchpoint flux and environmental parameters and (2) simulated and observed isotope data. In summary, intramolecular isotope analysis has an enormous potential to advance our knowledge about isotope fractionation mechanisms, plant ecophysiology, and paleoclimatology.

Acknowledgements

TW's work was carried out with funding from 'Formas – a Swedish Research Council for Sustainable Development' (2022-02833, Grant recipient: TW). MH-P's work was supported by the Swiss National Science Foundation (205492). We thank bioRxiv (Cold Spring Harbor Laboratory, NY, USA) for publishing preprints of the present paper (doi: 10.1101/2024.02.21.581384).

Competing interests

None declared.

Author contributions

Conceptualisation, visualisation, project administration, and development of isotope theory were done by TW. Investigation and writing were done by TW with input from MH-P, JY, and TN.

ORCID

Meisha Holloway-Phillips https://orcid.org/0000-0002-8353-3536
Totte Niittylä https://orcid.org/0000-0001-8029-1503
Thomas Wieloch https://orcid.org/0000-0001-9162-2291
Jun Yu https://orcid.org/0000-0001-5673-620X

Data availability

Isotope data used here were published previously (Wieloch *et al.*, 2018, 2022b). Climate data used here are publicly accessible (see the Materials and Methods section). Data derivatives supporting the findings of this study are available within the paper (see the Results section; Tables 3–7; Figs 3, 4, 6) and its supporting information (see Notes S2, S3; Tables S1–S6; Fig. S1).

References

Abtew W, Melesse AM. 2013. Chapter 5 – Vapor pressure calculation methods. In: *Evaporation and evapotranspiration*. Dordrecht, the Netherlands: Springer Verlag, 53–62. doi: 10.1007/978-94-007-4737-1.

Augusti A, Betson TR, Schleucher J. 2006. Hydrogen exchange during cellulose synthesis distinguishes climatic and biochemical isotope fractionations in tree rings. *New Phytologist* **172**: 490–499.

Badeck FW, Tcherkez G, Nogues S, Piel C, Ghashghaie J. 2005. Post-photosynthetic fractionation of stable carbon isotopes between plant organs – a widespread phenomenon. *Rapid Communications in Mass Spectrometry* **19**: 1381–1391.

Beguería S, Vicente-Serrano SM, Angulo-Martínez M. 2010. A multiscalar global drought dataset: the SPEIbase. *Bulletin of the American Meteorological Society* **91**: 1351–1356.

Betz GA, Gerstner E, Stich S, Winkler B, Welzl G, Kremmer E, Langebartels C, Heller W, Sandermann H, Ernst D. 2009. Ozone affects shikimate pathway genes and secondary metabolites in saplings of European beech (*Fagus sylvatica* L.) grown under greenhouse conditions. *Trees* **23**: 539–553.

Brunetti C, Savi T, Nardini A, Loreto F, Gori A, Centritto M. 2020. Changes in abscisic acid content during and after drought are related to carbohydrate mobilization and hydraulic recovery in poplar stems. *Tree Physiology* **40**: 1043–1057.

Cardi M, Chibani K, Cafasso D, Rouhier N, Jacquot J-P, Esposito S. 2011. Abscisic acid effects on activity and expression of barley (*Hordeum vulgare*) plastidial glucose-6-phosphate dehydrogenase. *Journal of Experimental Botany* **62**: 4013–4023.

Castiglia D, Cardi M, Landi S, Cafasso D, Esposito S. 2015. Expression and characterization of a cytosolic glucose 6 phosphate dehydrogenase isoform from barley (*Hordeum vulgare*) roots. *Protein Expression and Purification* **112**: 8–14.

Cernusak LA, Tcherkez G, Keitel C, Cornwell WK, Santiago LS, Knohl A, Barbour MM, Williams DG, Reich PB, Ellsworth DS *et al.* 2009. Why are non-photosynthetic tissues generally ^{13}C enriched compared with leaves in C_3

plants? Review and synthesis of current hypotheses. *Functional Plant Biology* **36**: 199–213.

Cossar JD, Rowell P, Stewart WDP. 1984. Thioredoxin as a modulator of glucose-6-phosphate dehydrogenase in a N_2-fixing cyanobacterium. *Microbiology* **130**: 991–998.

Craig H. 1953. The geochemistry of the stable carbon isotopes. *Geochimica et Cosmochimica Acta* **3**: 53–92.

Cuny HE, Rathgeber CBK, Frank D, Fonti P, Fournier M. 2014. Kinetics of tracheid development explain conifer tree-ring structure. *New Phytologist* **203**: 1231–1241.

Dietz K-J. 1985. A possible rate-limiting function of chloroplast hexosemonophosphate isomerase in starch synthesis of leaves. *Biochimica et Biophysica Acta* **839**: 240–248.

Dizengremel P. 2001. Effects of ozone on the carbon metabolism of forest trees. *Plant Physiology and Biochemistry* **39**: 729–742.

Esposito S, Carfagna S, Massaro G, Vona V, Di Martino Rigano V. 2001. Glucose-6-phosphate dehydrogenase in barley roots: kinetic properties and localisation of the isoforms. *Planta* **212**: 627–634.

Evans JR, Farquhar GD, Sharkey TD, Berry JA. 1986. Carbon isotope discrimination measured concurrently with gas exchange to investigate CO_2 diffusion in leaves of higher plants. *Australian Journal of Plant Physiology* **13**: 281–292.

Fan Y, van den Dool H. 2004. Climate Prediction Center global monthly soil moisture data set at 0.5° resolution for 1948 to present. *Journal of Geophysical Research: Atmospheres* **109**: D10102.

Farquhar GD. 1983. On the nature of carbon isotope discrimination in C_4 species. *Australian Journal of Plant Physiology* **10**: 205–226.

Farquhar GD, Ehleringer JR, Hubick KT. 1989. Carbon isotope discrimination and photosynthesis. *Annual Review of Plant Physiology and Plant Molecular Biology* **40**: 503–537.

Farquhar GD, O'Leary MH, Berry JA. 1982. On the relationship between carbon isotope discrimination and the intercellular carbon dioxide concentration in leaves. *Australian Journal of Plant Physiology* **9**: 121–137.

Farquhar GD, Richards RA. 1984. Isotopic composition of plant carbon correlates with water-use efficiency of wheat genotypes. *Australian Journal of Plant Physiology* **11**: 539–552.

Fedtke C. 1969. Intramolecular hydrogen transfer in isomerisation reactions of sugar phosphates in the Calvin cycle. In: Metzner H, ed. *Progress in photosynthesis research*. Tübingen, Germany: International Union of Biological Sciences, 1597–1603.

Gagen M, Battipaglia G, Daux V, Duffy J, Dorado-Liñán I, Hayles LA, Martínez-Sancho E, McCarroll D, Shestakova TA, Treydte K. 2022. Climate signals in stable isotope tree-ring records. In: Siegwolf RTW, Brooks JR, Roden J, Saurer M, eds. *Stable isotopes in tree tings: inferring physiological, climatic and environmental responses*. Cham, Switzerland: Springer, 537–579.

Gerhardt R, Stitt M, Heldt HW. 1987. Subcellular metabolite levels in spinach leaves: regulation of sucrose synthesis during diurnal alterations in photosynthetic partitioning. *Plant Physiology* **83**: 399–407.

Gilbert A, Robins RJ, Remaud GS, Tcherkez G. 2012. Intramolecular ^{13}C pattern in hexoses from autotrophic and heterotrophic C_3 plant tissues. *Proceedings of the National Academy of Sciences, USA* **109**: 18204–18209.

Grazi E, De Flora A, Pontremoli S. 1960. The inhibition of phosphoglucose isomerase by D-erythrose 4-phosphate. *Biochemical and Biophysical Research Communications* **2**: 121–125.

Grossiord C, Buckley TN, Cernusak LA, Novick KA, Poulter B, Siegwolf RTW, Sperry JS, McDowell NG. 2020. Plant responses to rising vapor pressure deficit. *New Phytologist* **226**: 1550–1566.

Hermes JD, Roeske CA, O'Leary MH, Cleland WW. 1982. Use of multiple isotope effects to determine enzyme mechanisms and intrinsic isotope effects. Malic enzyme and glucose 6-phosphate dehydrogenase. *Biochemistry* **21**: 5106–5114.

Hobbie EA, Werner RA. 2004. Intramolecular, compound-specific, and bulk carbon isotope patterns in C_3 and C_4 plants: a review and synthesis. *New Phytologist* **161**: 371–385.

Janzik I, Preiskowski S, Kneifel H. 2005. Ozone has dramatic effects on the regulation of the prechorismate pathway in tobacco (*Nicotiana tabacum* L. cv. Bel W3). *Planta* **223**: 20–27.

Klein Tank AMG, Wijngaard JB, Können GP, Böhm R, Demarée G, Gocheva A, Mileta M, Pashiardis S, Hejkrlik L, Kern-Hansen C *et al.* 2002. Daily dataset of 20th-century surface air temperature and precipitation series for the European Climate Assessment. *International Journal of Climatology* **22**: 1441–1453.

Kruckeberg AL, Neuhaus HE, Feil R, Gottlieb LD, Stitt M. 1989. Decreased-activity mutants of phosphoglucose isomerase in the cytosol and chloroplast of *Clarkia xantiana*. *The Biochemical Journal* **261**: 457–467.

Landi S, Nurcato R, De Lillo A, Lentini M, Grillo S, Esposito S. 2016. Glucose-6-phosphate dehydrogenase plays a central role in the response of tomato (*Solanum lycopersicum*) plants to short and long-term drought. *Plant Physiology and Biochemistry* **105**: 79–89.

Leavitt SW, Roden J. 2022. Isotope dendrochronology: historical perspective. In: Siegwolf RTW, Brooks JR, Roden J, Saurer M, eds. *Stable isotopes in tree rings: inferring physiological, climatic and environmental responses*. Cham, Switzerland: Springer, 3–20.

Leidreiter K, Kruse A, Heineke D, Robinson DG, Heldt H-W. 1995. Subcellular volumes and metabolite concentrations in potato (*Solanum tuberosum* cv. Désirée) leaves. *Botanica Acta* **108**: 439–444.

Li C, Wei M, Ge Y, Zhao J, Chen Y, Hou J, Cheng Y, Chen J, Li J. 2020. The role of glucose-6-phosphate dehydrogenase in reactive oxygen species metabolism in apple exocarp induced by acibenzolar-S-methyl. *Food Chemistry* **308**: 125663.

Liu J, Wang X, Hu Y, Hu W, Bi Y. 2013. Glucose-6-phosphate dehydrogenase plays a pivotal role in tolerance to drought stress in soybean roots. *Plant Cell Reports* **32**: 415–429.

Long SP. 1991. Modification of the response of photosynthetic productivity to rising temperature by atmospheric CO_2 concentrations: has its importance been underestimated? *Plant, Cell & Environment* **14**: 729–739.

Lu X, Zhang L, Shen L. 2019. Meteorology and climate influences on tropospheric ozone: a review of natural sources, chemistry, and transport patterns. *Current Pollution Reports* **5**: 238–260.

McCulloh KA, Domec J-C, Johnson DM, Smith DD, Meinzer FC. 2019. A dynamic yet vulnerable pipeline: integration and coordination of hydraulic traits across whole plants. *Plant, Cell & Environment* **42**: 2789–2807.

McDowell N, Pockman WT, Allen CD, Breshears DD, Cobb N, Kolb T, Plaut J, Sperry J, West A, Williams DG *et al.* 2008. Mechanisms of plant survival and mortality during drought: why do some plants survive while others succumb to drought? *New Phytologist* **178**: 719–739.

Mitchell PJ, O'Grady AP, Tissue DT, White DA, Ottenschlaeger ML, Pinkard EA. 2013. Drought response strategies define the relative contributions of hydraulic dysfunction and carbohydrate depletion during tree mortality. *New Phytologist* **197**: 862–872.

Mueller EP, Wu F, Sessions AL. 2022. Quantifying Isotopologue Reaction Networks (QIRN): a modelling tool for predicting stable isotope fractionations in complex networks. *Chemical Geology* **610**: 121098.

Nilsson MB, Dåbakk E, Korsman T, Renberg I. 1996. Quantifying relationships between near-infrared reflectance spectra of lake sediments and water chemistry. *Environmental Science & Technology* **30**: 2586–2590.

Noltmann EA. 1972. 9 Aldose-ketose isomerases. In: Boyer PD, ed. *The enzymes*. New York, NY, USA: Academic Press, 271–354.

Noronha H, Silva A, Dai Z, Gallusci P, Rombolà AD, Delrot S, Gerós H. 2018. A molecular perspective on starch metabolism in woody tissues. *Planta* **248**: 559–568.

Parr CW. 1956. Inhibition of phosphoglucose isomerase. *Nature* **178**: 1401.

Preiser AL, Fisher N, Banerjee A, Sharkey TD. 2019. Plastidic glucose-6-phosphate dehydrogenases are regulated to maintain activity in the light. *Biochemical Journal* **476**: 1539–1551.

R Core Team. 2021. *R: a language and environment for statistical computing*. Vienna, Austria: R Foundation for Statistical Computing. [WWW document] URL https://www.R-project.org/.

Roden JS, Lin G, Ehleringer JR. 2000. A mechanistic model for interpretation of hydrogen and oxygen isotope ratios in tree-ring cellulose. *Geochimica et Cosmochimica Acta* **64**: 21–35.

Roeske CA, O'Leary MH. 1984. Carbon isotope effects on the enzyme-catalyzed carboxylation of ribulose bisphosphate. *Biochemistry* **23**: 6275–6284.

Rose IA, O'Connell EL. 1961. Intramolecular hydrogen transfer in the phosphoglucose isomerase reaction. *The Journal of Biological Chemistry* **236**: 3086–3092.

Ross GJ. 2015. Parametric and nonparametric sequential change detection in R: the CPM package. *Journal of Statistical Software* **66**: 1–20.

Salas M, Vinuela E, Sols A. 1965. Spontaneous and enzymatically catalyzed anomerization of glucose 6-phosphate and anomeric specificity of related enzymes. *Journal of Biological Chemistry* **240**: 561–568.

Schleucher J, Vanderveer P, Markley JL, Sharkey TD. 1999. Intramolecular deuterium distributions reveal disequilibrium of chloroplast phosphoglucose isomerase. *Plant, Cell & Environment* **22**: 525–533.

Schmiege SC, Heskel M, Fan Y, Way DA. 2023. It's only natural: plant respiration in unmanaged systems. *Plant Physiology* **192**: 710–727.

Schubert BA, Jahren AH. 2012. The effect of atmospheric CO_2 concentration on carbon isotope fractionation in C_3 land plants. *Geochimica et Cosmochimica Acta* **96**: 29–43.

Sharkey TD, Berry JA, Raschke K. 1985. Starch and sucrose synthesis in *Phaseolus vulgaris* as affected by light, CO_2, and abscisic acid. *Plant Physiology* **77**: 617–620.

Sharkey TD, Weise SE. 2016. The glucose 6-phosphate shunt around the Calvin–Benson cycle. *Journal of Experimental Botany* **67**: 4067–4077.

Stincone A, Prigione A, Cramer T, Wamelink MM, Campbell K, Cheung E, Olin-Sandoval V, Gruning N, Kruger A, Tauqeer Alam M *et al.* 2015. The return of metabolism: biochemistry and physiology of the pentose phosphate pathway. *Biological Reviews of the Cambridge Philosophical Society* **90**: 927–963.

Szecowka M, Heise R, Tohge T, Nunes-Nesi A, Vosloh D, Huege J, Feil R, Lunn J, Nikoloski Z, Stitt M *et al.* 2013. Metabolic fluxes in an illuminated *Arabidopsis* rosette. *Plant Cell* **25**: 694–714.

Thalmann M, Santelia D. 2017. Starch as a determinant of plant fitness under abiotic stress. *New Phytologist* **214**: 943–951.

Topper YJ. 1957. On the mechanism of action of phosphoglucose isomerase and phosphomannose isomerase. *Journal of Biological Chemistry* **225**: 419–425.

Tsamir-Rimon M, Ben-Dor S, Feldmesser E, Oppenhimer-Shaanan Y, David-Schwartz R, Samach A, Klein T. 2021. Rapid starch degradation in the wood of olive trees under heat and drought is permitted by three stress-specific beta amylases. *New Phytologist* **229**: 1398–1414.

Ubierna N, Holloway-Phillips M-M, Farquhar GD. 2022. Scaling from fluxes to organic matter: interpreting ^{13}C isotope ratios of plant material using flux models. *New Phytologist* **236**: 2003–2008.

Vicente-Serrano SM, Beguería S, López-Moreno JI. 2010. A multiscalar drought index sensitive to global warming: the standardized precipitation evapotranspiration index. *Journal of Climate* **23**: 1696–1718.

Wacker A. 2022. *Leaf sucrose shows no nighttime ^{2}H-depletion despite the degradation of strongly ^{2}H-depleted starch.* Master thesis, University of Basel, Basel, Switzerland.

Wang H, Yang L, Li Y, Hou J, Huang J, Liang W. 2016. Involvement of ABA- and H_2O_2-dependent cytosolic glucose-6-phosphate dehydrogenase in maintaining redox homeostasis in soybean roots under drought stress. *Plant Physiology and Biochemistry* **107**: 126–136.

Wang X, Ruan M, Wan Q, He W, Yang L, Liu X, He L, Yan L, Bi Y. 2020. Nitric oxide and hydrogen peroxide increase glucose-6-phosphate dehydrogenase activities and expression upon drought stress in soybean roots. *Plant Cell Reports* **39**: 63–73.

Ward JH. 1963. Hierarchical grouping to optimize an objective function. *Journal of the American Statistical Association* **58**: 236–244.

Wendt UK, Wenderoth I, Tegeler A, Von Schaewen A. 2000. Molecular characterization of a novel glucose-6-phosphate dehydrogenase from potato (*Solanum tuberosum* L.). *The Plant Journal* **23**: 723–733.

Wieloch T. 2021. A cytosolic oxidation–reduction cycle in plant leaves. *Journal of Experimental Botany* **72**: 4186–4189.

Wieloch T. 2022. High atmospheric CO_2 concentration causes increased respiration by the oxidative pentose phosphate pathway in chloroplasts. *New Phytologist* **235**: 1310–1314.

Wieloch T, Augusti A, Schleucher J. 2022a. Anaplerotic flux into the Calvin–Benson cycle. Hydrogen isotope evidence for *in vivo* occurrence in C_3 metabolism. *New Phytologist* **234**: 405–411.

Wieloch T, Augusti A, Schleucher J. 2023. A model of photosynthetic CO_2 assimilation in C_3 leaves accounting for respiration and energy recycling by the plastidial oxidative pentose phosphate pathway. *New Phytologist* **239**: 518–532.

Wieloch T, Ehlers I, Yu J, Frank D, Grabner M, Gessler A, Schleucher J. 2018. Intramolecular ^{13}C analysis of tree rings provides multiple plant ecophysiology signals covering decades. *Scientific Reports* **8**: 5048.

Wieloch T, Grabner M, Augusti A, Serk H, Ehlers I, Yu J, Schleucher J. 2022b. Metabolism is a major driver of hydrogen isotope fractionation recorded in tree-ring glucose of *Pinus nigra*. *New Phytologist* **234**: 449–461.

Wieloch T, Sharkey TD, Werner RA, Schleucher J. 2022c. Intramolecular carbon isotope signals reflect metabolite allocation in plants. *Journal of Experimental Botany* **73**: 2558–2575.

Wieloch T, Werner RA, Schleucher J. 2021. Carbon flux around leaf-cytosolic glyceraldehyde-3-phosphate dehydrogenase introduces a ^{13}C signal in plant glucose. *Journal of Experimental Botany* **72**: 7136–7144.

Supporting Information

Additional Supporting Information may be found online in the Supporting Information section at the end of the article.

Fig. S1 Air vapour pressure deficit of the growing season and March–July precipitation over the period from 1961 to 1995 in the Vienna basin.

Notes S1 Materials and Methods (expanded).

Notes S2 Hydro-carbon isotope fractionation from 1961 to 1980.

Notes S3 Estimated deuterium fractionation due to shifts of the phosphoglucose isomerase reaction.

Table S1 Shapiro–Wilk normality test.

Table S2 F and T test.

Table S3 Pearson's correlations between Δ_i' and ε_{met} series of the period from 1983 to 1995.

Table S4 Components of variance in Δ_i' series.

Table S5 Pearson's correlation coefficients and associated levels of significance of ε_{met}-climate relationships for the period from 1983 to 1995.

Table S6 Linear regression model of $\varepsilon_{met\ (H1)}$ as function of growing season air vapour pressure deficit and March–July precipitation.

Please note: Wiley is not responsible for the content or functionality of any Supporting Information supplied by the authors. Any queries (other than missing material) should be directed to the *New Phytologist* Central Office.